https://doi.org/10.5194/egusphere-2026-3489
Preprint. Discussion started: 14 July 2026

Climatic, tectonic and landslide-dam signals preserved in alluvial terraces of the Naryn Basin, Kyrgyzstan

Andreas Ruby[1], Taylor F. Schildgen[1,2], Fergus McNab[1,2], Andrew D. Wickert[1,3,4], Apolline Mariotti[1,5], Hella Wittmann[1], Bolot Moldobekov[6], Thomas Kolb[7], Markus Fuchs[7]

[1]GFZ Helmholtz Center for Geosciences, 14473 Potsdam, Germany
[2]Institute for Geosciences, University of Potsdam, 14476 Potsdam, Germany
[3]Department of Earth & Environmental Sciences, University of Minnesota, Minneapolis 55455, MN, USA
[4]Saint Anthony Falls Laboratory, University of Minnesota, Minneapolis 55414, MN, USA
[5]Trinity College, Dublin 2, Ireland
[6]Central Asia Institute of Applied Geoscience, 720027 Bishkek, Kyrgyzstan
[7]University of Gießen, 35390 Gießen, Germany

Correspondence to: Andreas Ruby (andreas.ruby@gfz.de)

Abstract. Fluvial terraces can act as geomorphic markers of past environmental change. Although they are commonly interpreted in the context of a single driver, multiple climatic and/or tectonic processes may occur simultaneously in nature. Here, we test our ability to interpret terrace sequences with potentially complex formation histories by studying the Naryn Basin in the central Tien Shan, where glacial–interglacial cycles affected land-surface processes, numerous active faults accommodate crustal shortening, and a large landslide temporarily dammed a lake. We investigate the relative contribution of these terrace-formation drivers by mapping terrace profiles, providing new constraints on the terrace chronology, and numerically simulating terrace formation in response to climate change and lake drainage. Tributary terrace profiles record local deformation in response to faults and a regional concave-up pattern that could be explained by lacustrine sedimentation and subsequent base-level fall induced by lake drainage. Terrace ages cluster between 15 and 20 ka, correlating with both deglaciation following the last glacial maximum and lake drainage. Our modelling, together with the spatial distribution of modelled terraces, indicates that lake drainage had a strong, but spatially restricted impact on river long-profile evolution, whereas Pleistocene climate triggered regional terrace formation. By integrating numerical modelling of alluvial river long-profile evolution with detailed mapping and geochronology, we present a robust approach to establish direct links between environmental change and the resulting terrace record.

1 Introduction

Alluvial rivers continuously adjust their slopes, channel widths and sediment-transport rates to changes in water discharge, sediment supply, base level, and/or uplift rates (Mackin, 1948; Lane, 1955; Ouchi, 1985; Tofelde et al., 2019; Merritts et al., 1994). When a river incises into its formerly deposited floodplain, a fluvial terrace may form, preserving the prior landscape at the time that it was disturbed (Bridgland & Westaway, 2008; Bull, 1991; Merritts et al., 1994; Pazzaglia, 2013). An implication is that river terraces may record information about past environmental or tectonic change. Indeed, several studies have explored alluvial river responses to climatic or tectonic forcing (e.g., Huntington, 1907; Hancock et al., 1999; Poisson & Avouac, 2004; Viveen et al., 2014; Scherler et al., 2015). However, relatively few studies have considered complications that arise due to channel network configurations (McNab et al., 2025; Benda et al., 2004; Savi et al., 2020) or multiple terrace-forming

https://doi.org/10.5194/egusphere-2026-3489
Preprint. Discussion started: 14 July 2026

processes acting simultaneously (e.g., Fernandes et al., 2026; Ruby et al., 2026; Ma et al., 2023; Hetzel et al., 2006; Hassenruck-Gudipati et al., 2022; Hu et al., 2012). Nevertheless, there is no established approach for distinguishing between and quantifying terrace-formation mechanisms in complex settings.

The Tien Shan in Central Asia hosts complex river networks that flow through intermontane basins and are flanked by flights of fluvial terraces. This region provided one of the earliest links between a dated terrace sequence and Late Pleistocene climate oscillations (Molnar et al., 1994). In the following years, paleo-climatic interpretations that emerged from terrace studies in the Eastern Tien Shan continued to explain terrace formation with broad-scale climate changes during glacial-interglacial transitions (Lu et al., 2010; Lu et al., 2014; Gong et al., 2014; Yang et al., 2013), whereas individuals estimated past water discharge from terrace slopes (Poisson & Avouac, 2004) or emphasized the past glacial impact on valley geometry and fluvial response to climate changes (Malatesta et al., 2018). Although the Westerlies dominate modern precipitation throughout most of the Tien Shan, questions remain about changes in the source, amount, and seasonality of precipitation on orbital timescales throughout the region (Cheng et al., 2012; Cheng et al., 2016). Moreover, trace elements and $\delta^{13}C$ in speleothems indicate contrasting regional hydrology for the western and central Tien Shan compared to global climate patterns (Cheng et al., 2016). Consequently, the evolution of the regional landscape—and the accompanying fluvial response to both global and regional climate—remains poorly constrained, and extrapolating the few interpretations from the eastern Tien Shan to the west cannot be justified.

Research on alluvial terraces in the tectonically active central Tien Shan has focused instead on using terraces as geomorphic markers to quantify deformation along reverse and strike-slip faults (Thompson et al., 2002; Hubert-Ferrari et al., 2005; Scharer et al., 2006; Selander et al., 2012; Cording et al., 2014; Goode et al., 2014; Saint-Carlier et al., 2016; Mackenzie et al., 2018; Campbell et al., 2019; Coddington & Burgette 2020). Seismic activity in the Kyrgyz Tien Shan was probably also the trigger of one of the largest landslides known to have occurred in Central Asia, the Beshkiol landslide (Losen et al. 2024). At ~25 ka, a section of a mountain range bounding the Naryn Basin, in the central Kyrgyz Tien Shan, collapsed and dammed the Naryn River to form two consecutive lakes, as recorded by lacustrine sediments and paleoshorelines mapped upstream from the landslide (Losen et al., 2024; Losen, 2024). Terraces cut into and below the lake sediments record the re-establishment of the fluvial network after breaching of the landslide dam(s).

Considering that the Naryn Basin has been subject to (i) tectonic forcing via slip along active faults, (ii) Pleistocene climate oscillations including glacial advances in the headwaters, and (iii) two paleo-lakes in the last 25 ky, the terraces that now exist throughout the Naryn Basin may have formed in response to one or multiple drivers. Recent modelling of the long-profile evolution of an alluvial river in Southern Patagonia illustrated how it may be possible to distinguish among terraces generated by cyclical changes in the sediment and water supply from those generated due to base-level cycles (Ruby et al., 2026). However, that study considered a relatively simple setting, with no significant tributaries supplying water or sediment along the trunk stream. Disentangling the relative importance of terrace formation drivers within the context of the Naryn River network is a more complex endeavor; how terrace formation may propagate upstream and downstream through linked tributaries, and how the network configuration affects these signals, is difficult to predict without explicit modeling of the full network (e.g., McNab et al., 2025).

https://doi.org/10.5194/egusphere-2026-3489
Preprint. Discussion started: 14 July 2026

We approach this challenge by, first, conceptually summarizing potential terrace extents and profiles in response to three hypothesized mechanisms of terrace formation: (1) differential uplift across faults; (2) orbital scale climate changes that alter water and sediment supply to the river valleys; and (3) rapid base-level fall following lake drainage. We then present alluvial terrace profiles and newly acquired terrace ages along the trunk of the Naryn River and its tributaries. Ages comprise both exposure ages of individual boulders and a depth profile derived from in-situ produced ^{10}Be, as well as depositional ages of sediment from luminescence dating. Finally, we perform numerical modelling of the fluvial network's long-profile evolution to gain insights into the spatial extent and geometric characteristics of fluvial terrace formation in response to cyclic climate changes and rapid base-level fall associated with lake drainage. We conclude by assessing the relative contribution of the various potential drivers to the formation of terrace sequences in the Naryn Basin.

2 Study Area

The Naryn River drains ~60.000 km^2 of the central Tien Shan, traversing several narrow intermontane basins before reaching the Naryn Basin (Figure 1). There, the main trunk stream as well as most tributaries host sequences of alluvial cut-and-fill terraces that consist primarily of fluvial gravels, overlain by fine-grained sediment (Thompson et al., 2002). Previous studies dating these terraces derived late Quaternary ages and

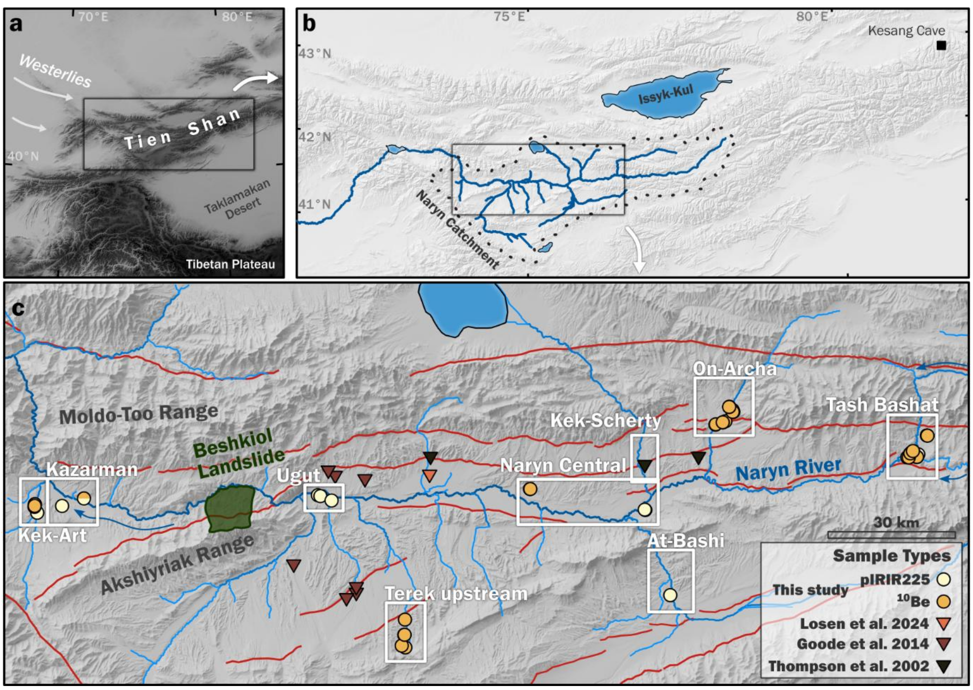

Figure 1: Map overview of the study region. (a) relief map of the Tien Shan located in the westerlies zone. (b) Naryn River and its catchment (dotted line; until it enters a bedrock gorge downstream of Kazarman) in the central Tien Shan. The black square is the location of the Kesang cave paleo-climate archive. (c) sample locations within the Naryn Basin. Bright yellow circles: luminescence samples; orange circles: ^{10}Be exposure age samples. Triangular samples (red and dark brown): literature samples mentioned in text. The Beshkiol Landslide: green polygon on the northern slope of the Akshiyriak Range. Red lines: selected major faults from the AFEAD database (Zelenin et al., 2022).

https://doi.org/10.5194/egusphere-2026-3489
Preprint. Discussion started: 14 July 2026

calculated fault-slip rates, based on both luminescence and ^{14}C in organic material (Thompson et al. 2002; Goode et al., 2014).

2.1 Paleoclimate

Paleoclimate proxies across the region yield apparently contrasting interpretations regarding past changes in precipitation. Variation in $\delta^{18}O$ from stalagmites in the Kesang Cave (around 600 km east of the Naryn Basin; Figure 1b) show a 23-ky orbitally paced cyclicity linked to the interplay of the Asian summer monsoon and the Westerlies, but the precise effects on local precipitation remain unclear. For example, $\delta^{13}C$ and trace elements in the same record indicate wetter glacials and drier interglacials (Cheng et al., 2012; Cheng et al., 2016), whereas loess profiles in the region show strongest deposition in glacial periods, suggesting dry and windy glacials (Fitzsimmons et al., 2018; Youn et al., 2014; Song et al., 2018; Li et al., 2018; Kang et al., 2015). Similarly, increased grass and decreased tree pollen in glacially associated terrace deposits indicate colder and drier glacial climates (Grigina & Fortuna, 1981). The moraine record, although overall imprecisely dated and reflecting changes in both temperature and precipitation, seems to mimic global climate dynamics, with, for example, ice advances during MIS 5, 3, and (especially) 2 (Abramowski, et al., 2006; Blomdin et al., 2016; Koppes et al., 2008; Narama et al., 2007, 2009; Zhao et al., 2010; Zech, 2012). In places, abandonment of fluvial terraces has been associated with glacial periods – an observation used to argue for high discharge during or shortly after peak glacials, either due to strong pulses of glacial meltwater (Cordier et al., 2017) or very limited evaporation (Zhang et al., 2023).

2.2 Geomorphic features

At 25 ka, near the western limit of the Naryn Basin, the northern slopes of the Akshiyriak Range failed and formed the Beshkiol landslide, the largest known landslide in Central Asia (8-12 km^3; Figure 1c; Losen et al., 2024; Losen 2024; Korup et al., 2006; Strom, 1998). Consequent damming of the Naryn River created a lake that persisted for ~10 ky, associated with up to 70 m of sediment deposition (the Erkin Formation), before the landslide dam collapsed, inducing a catastrophic lake drainage (Losen et al., 2024; Losen 2024). A second, smaller landslide occurred shortly after, around 14 ka, damming another lake that persisted for ~8 ky. In this second lake, the Sultan Formation accumulated with a maximum thickness of 20 m (Losen et al., 2024; Losen 2024). Both the Erkin and Sultan formations mainly consist of laminated silt and clay with lenses of sand and clast-supported gravels. These coarse lenses are interpreted as deposits of occasional bottom dense debris flows, whereas ripples are ascribed to reworking by bottom currents (Losen et al., 2024).

As well as the distribution of lacustrine deposits, Losen et al. (2024) mapped paleo-shorelines throughout the basin and correlated their elevations to those of the landslide body. They identified two relatively long-lived lake levels (1st lake 1850 m; 2nd lake 1720 m; Figure 2) with respective lake volumes of ~121 km^3 and ~27 km^3. Features at 1977 m (41.300°N 75.153°E) and 2200 m (41.190°N 74.980°E; 41.200°N 74.695°E; 41.548°N 74.853°E) – 450 m higher than the Beshkiol landslide body – might represent older paleo-shorelines. A lake surface at these elevations would overtop the Beshkiol landslide, and so would probably require a larger dam farther downstream. There is, however, no evidence for such a dam, nor for the continuation of paleo-shorelines

https://doi.org/10.5194/egusphere-2026-3489
Preprint. Discussion started: 14 July 2026

downstream of the Akshiyriak Range. The significance of these higher, potential paleo-shoreline features therefore remains unclear.

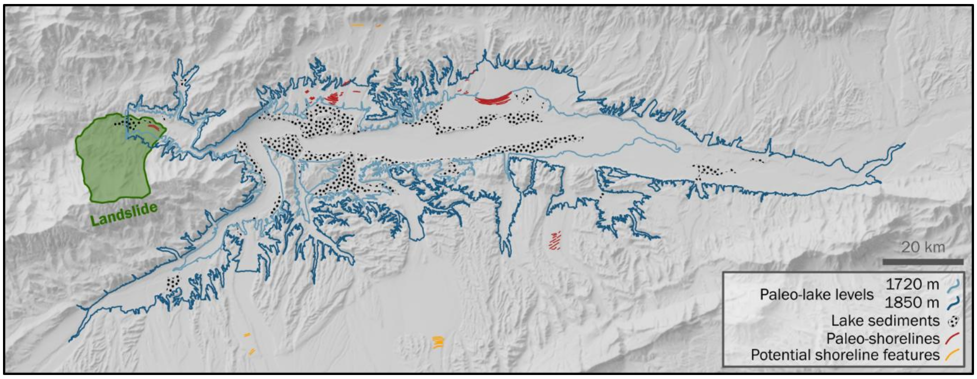

Figure 2: Potential extents of the two paleo lakes formed in response to the Beshkiol landslide dam. Additionally, paleo-shorelines and lacustrine sediments mapped by Losen et al. (2024) and potential other shoreline features mapped by us are shown.

3 Concepts of fluvial terrace formation

~~The terraces in the Naryn Basin have been used primarily to reconstruct late Quaternary fault slip rates. However, in the geomorphological context of climatic, tectonic and lake-level change, the actual drivers of their formation have not been directly addressed.~~ Here, we introduce three end-member mechanisms that could explain the formation of these terraces.

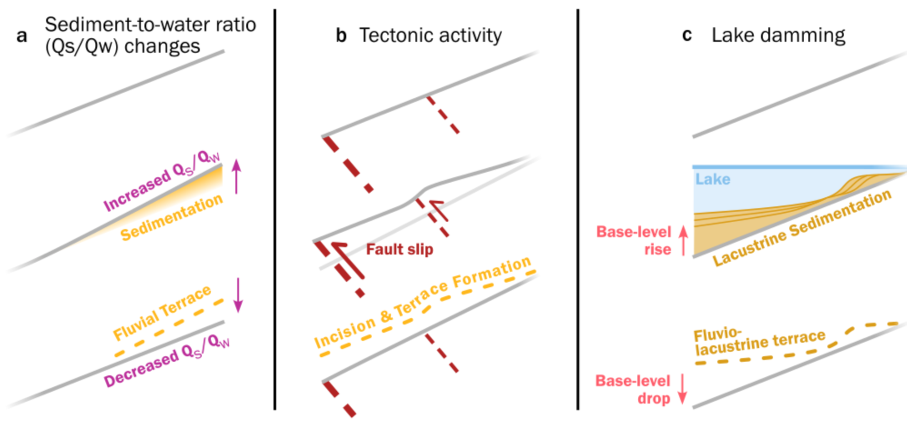

Figure 3: Schematic long-profile illustration of terrace formation. (a) climate induced changes in the sediment-to-water supply ratio (Q_s/Q_w), (b) tectonic activity and (c) lake damming on terrace formation. Grey lines represent the river profile and the dashed yellow-orange lines show the resulting theoretical terrace profiles. Note that for (b) the thin red dashed line represents localized fault deformation, whereas the thick red dashed line represents a change in regional rock-uplift rate that results in a steeper channel profile.

3.1 Cyclic Climate Forcing

As the slope of an alluvial channel is affected by the ratio of sediment to water supply (e.g., Howard, 1982; Lane, 1955; Paola et al., 1992; Tofelde et al., 2019; Wickert & Schildgen, 2019), changes in either will cause

https://doi.org/10.5194/egusphere-2026-3489
Preprint. Discussion started: 14 July 2026

channels to adjust their slopes via aggradation or incision (e.g., Parker et al., 1998; van den Berg van Saparoea and Postma, 2008; Tofelde et al., 2019). For example, a transient increase in sediment supply or decrease in water supply at a channel head will trigger aggradation and channel steepening that will propagate downstream. Subsequent incision, driven by increased water supply or decreased sediment supply, will then produce terraces that are steeper than the modern channel (Figure 3a; McNab et al., 2023; Ruby et al., 2026). Whereas climate impacts on water supply are closely linked to variations in precipitation, climate-induced changes in sediment supply can be harder to predict, as both temperature and precipitation can affect processes controlling sediment production and down-slope transport (Bridgland & Westaway, 2008; Hancock et al., 1999; Cordier et al., 2017; Mair et al., 2020; Marshall et al., 2015; Penprase et al., 2025; Roda-Boluda, et al., 2023; Torres Acosta et al., 2015; Vandenberghe, 2003, 2008). Regardless of the exact trigger, we consider diagnostic aspects of a terrace formed due to a change in Q_s/Q_w to be (1) slopes similar to or steeper than the modern profile, and (2) terrace extents that propagate downstream from channel heads.

3.2 Tectonic Forcing

If an alluvial river experiences an increase in tectonic uplift rate, its channel will become steeper and its concavity will decrease (Harvey & Wells, 1987; Stokes & Mather, 2000; Wickert & Schildgen, 2019). Hence, terraces abandoned during subsequent incision tend to have a lower slope compared to the modern channel. Different patterns can emerge if a river passes over a fault accommodating differential uplift, as the fault activity will deform pre-existing fluvial terraces (Figure 3b; Viveen et al., 2014; Saint-Carlier et al., 2016; Ouchi, 1985; Holbrook & Schumm 1999). Whereas wavelengths of deformation from individual faults can reach several tens of kilometers (O'Connell & Turner, 2023; McGregor & Onderdonk, 2021), they commonly span only a few km in the Tien Shan (Molnar et al., 1994; Thompson et al., 2002; Hubert-Ferrari et al., 2005; Scharer et al., 2006; Selander et al., 2012).

3.3 Lake Damming and Breaching

When a channel enters a lake, the location and nature of lacustrine deposits depend on the fluvial transport mode. Coarse grain sizes traveling as bedload are typically deposited proximally, whereas finer grain sizes travel in suspension over larger distances. Resulting depositional forms consist mostly of fan deltas with topsets and foresets where tributaries enter the lake and hemipelagic mud layers in deeper, more distal lake areas (see Figure 3c; Rust, 1982; Chen et al., 2016; Colman et al., 2003; Wells et al., 1999). However, recently formed lakes occupying a former fluvial valley could focus sediment transport as turbidity currents to submerged valley bottoms, and thereby facilitate more distal coarse-grained sediment transfer into deeper water (Rust, 1982). If a dam impounding the lake breaches, the lake will drain, exposing the recently deposited sediments. The channel will incise through these sediments while returning to its original, steeper slope. Remnants of the former lake bottom could remain as terraces along the main channel and the downstream tributary reaches while the upstream segments remain unaffected.

https://doi.org/10.5194/egusphere-2026-3489
Preprint. Discussion started: 14 July 2026

4 Methods

4.1 Terrace mapping and profile extraction

To better understand spatial patterns of terrace formation, terrace sequences, and terrace-profile geometries, we mapped terrace and channel elevations along major tributaries in the Naryn Basin. We extracted elevations from the freely available, 30-m resolution FABDEM (Forest and Buildings removed DEM; Hawker et al., 2022), which is derived from the 30-m resolution Copernicus DEM.

4.2 Geochronology

We constrained the timing of sediment aggradation and terrace abandonment with 37 cosmogenic nuclide exposure ages (using in-situ produced ^{10}Be from individual boulders or amalgamated pebble samples and from one depth profile) and 10 luminescence ages derived from K-feldspar using post-infrared infrared stimulated luminescence measured at 225°C (pIRIR225).

4.2.1 Cosmogenic Nuclide Exposure Dating

When sampling for ^{10}Be surface exposure dating, we targeted flat surfaces with sample sites at least several 10s of meters away from the terrace edge or from visible bumps, gullies or faults. With a hammer and chisel, we sampled the upper few centimeters of boulders and cobbles of quartz-bearing lithologies. When these larger clasts were not available, we instead collected amalgamated quartz pebble samples of more than 100 individual pebbles. For all sample types, we preferred smooth, rounded geometries suggesting fluvial transport. Sampled boulders were generally well rounded, smooth, and hard, suggesting minimal weathering.

We crushed and sieved samples to obtain the 250-500 μm fraction. We extracted ^{10}Be from pure quartz in the HELGES laboratory at GFZ Helmholtz Centre for Geosciences (Potsdam, Germany) following the protocol of von Blanckenburg et al. (2004) and spiked samples and blanks with between 155 and 164 μg of ^{9}Be carrier. We measured ^{10}Be /^{9}Be ratios at the Cologne AMS facility (Cologne, Germany), normalized results to standards of Nishiizumi et al. (2007), which are consistent with a half-life of ^{10}Be of $1.36 \pm 0.07 \times 10^{6}$ yr, and converted them into ^{10}Be concentrations after subtracting blank-specific ratios and using the ^{9}Be carrier concentrations.

We calculated exposure ages using the CREp online calculator (Martin et al., 2017) based on a quartz density of 2.6 g/cm^3 and sample thicknesses measured in the field. We corrected for topographic shielding via the *toposhielding* algorithm in "TopoToolbox" using an azimuth spacing of 10° and a zenith spacing of 5° (Schwanghart & Scherler, 2014). We assumed weathering and erosion rates to be zero based on the roundness and hardness of most boulders. We additionally corrected ^{10}Be concentrations with values from blanks that were processed simultaneously in the lab. Due to the absence of any local reference production-rate site, we use the global production rate of 4.11 ± 0.19 at/g/yr at sea level, the Lal-Stone scaling scheme, and the ERA40 atmosphere model.

For the conversion of calculated sample ages to terrace abandonment ages, we consider that age clusters provide a higher level of confidence compared to individual ages, and that terrace surface ages should get progressively older as elevation above the modern river increases. In some cases, highly dispersed ages from an individual

https://doi.org/10.5194/egusphere-2026-3489
Preprint. Discussion started: 14 July 2026

surface or set of surfaces necessitated more nuanced interpretations. We will outline our specific reasoning for each of these cases individually in the Results.

4.2.2 Post-infrared infrared stimulated luminescence (pIRIR225) dating

We collected ten samples for luminescence dating, including eight samples from fluvial terrace successions, where we sampled silty to sandy fine-grained lenses either from within fluvial gravels (22-KG-15, 22-KG-17, 22-KG-27, 22-KG-37, and 22-KG-38) or from fine-grained units overlying fluvial gravels (22-KG-13, 22-KG-40, and 22-KG-45). In addition, we collected two samples from lacustrine sediments (22-KG-08 and 22-KG-23). Samples were collected by hammering opaque, 6-cm diameter, 12-cm long metal tubes into the outcrop, and after digging out the tubes, sealing both ends with opaque plastic caps.

We extracted coarse-grain K-feldspar (90–200 µm) from the middle sections of the sample tubes at the luminescence laboratory of Justus Liebig University Giessen under subdued amber-light conditions and followed standard procedures of sample preparation (Fuchs et al., 2010): after wet sieving to the target grain-size fraction, we removed carbonates and organic matter using 10% HCl and 10% H_2O_2, respectively. We finally isolated the K-feldspar-rich fraction by heavy-liquid density separation with lithium polytungstate (2.58 g/cm^3 and 2.63 g/cm^3). We did not apply any HF-etching.

We carried out luminescence measurements at Justus Liebig University Giessen using automated Freiberg Instruments Lexsyg Smart readers equipped with internal ^{90}Y/^{90}Sr β-sources and infrared LEDs (850 nm, 150 mW/cm^2). The emitted signal was detected with a Hamamatsu H7360 photomultiplier tube through an AHF BrightLine HC414/46 and Schott BG39 filter combination, centered at approximately 410 nm. We measured samples using the pIRIR225 protocol (Thomsen et al., 2008; Buylaert et al., 2009), with a readout time of 300 s and following the recommendations given by Colarossi et al. (2018). We derived equivalent doses (DE) for individual aliquots from single saturating exponential fits to the dose-response curves, using the first 5 s of the IRSL signal after subtraction of a background obtained from the last 100 s. We accepted only aliquots with recycling ratios between 0.9 and 1.1, recuperation ≤ 5% of the natural sensitivity-corrected signal, and signal intensities at least three times the background. We calculated final sample DE values using the Minimum Age Model (Galbraith et al., 1999) to account for incomplete bleaching, which is expected particularly in fluvial settings.

We determined environmental dose rates from homogenized bulk sediment collected within a 30 cm radius around each sampling point and calculated it based on the µDose system (Tudyka et al., 2020, Kolb et al., 2022). We applied water contents of 15 ± 5% based on present-day moisture measurements and adjusted for site-specific sedimentological and geomorphological conditions. We calculated cosmic dose rates following Prescott and Hutton (1994) using the *calc_CosmicDoseRate* function of the R package “Luminescence” (Kreutzer et al., 2012) and performed data processing using modified routines of the R package “Luminescence”, and obtained final dose rates and age estimates with DRAC v1.2 (Durcan et al., 2015) using the conversion factors of Guérin et al. (2011). Fading tests on selected samples yielded generally low fading rates of ~1–1.5% per decade. Therefore, we did not apply any fading correction.

https://doi.org/10.5194/egusphere-2026-3489
Preprint. Discussion started: 14 July 2026

We interpreted the resulting luminescence ages as depositional ages of the sampled fine-grained units. For the lacustrine samples 22-KG-08 and 22-KG-23, these ages provide minimum constraints on lake formation. In the terrace successions, ages from fine-grained units overlying fluvial gravels (22-KG-13, 22-KG-40, and 22-KG-45) provide minimum ages for the underlying gravels and, where appropriate, also for terrace abandonment. Ages from fine-grained units intercalated within fluvial deposits (22-KG-15, 22-KG-17, 22-KG-27, 22-KG-37, and 22-KG-38) provide maximum age constraints on terrace abandonment.

4.3 Modelling terrace formation

4.3.1 Theory

We apply a numerical model originally developed by Wickert & Schildgen (2019) for single-valley segments and implemented in a network framework by McNab et al. (2025) that predicts long-profile evolution of transport-limited, gravel-dominated valleys. It combines mass conservation (Exner, 1925), a sediment-transport formula following Meyer-Peter and Müller (1948) and updated by Wong and Parker (2006), an assumption of equilibrium channel width (Parker 1978), and a grain-size-dependent Manning-Strickler expression for bed roughness (Parker 1991, Clifford et al., 1992). The governing equation for each channel segment is:

$$\frac{\partial z}{\partial t} = \frac{k_{Q_s} I}{\mathbb{S}^{\frac{7}{6}} B (1 - \lambda_p)} \frac{\partial}{\partial x} \left(Q_w \frac{\partial z}{\partial x} \left| \frac{\partial z}{\partial x} \right|^{\frac{1}{6}} \right) + \zeta \qquad (1)$$

with valley-floor elevation z, time t, intermittency I (fraction of time at the specified discharge), channel sinuosity $\mathbb{S}$, sediment porosity λ_p and down-valley distance x. k_{Qs} is a sediment-transport-efficiency coefficient, with a value of approximately 0.041 (Wickert & Schildgen, 2019). It combines physical constants, a coefficient linking grain size and clustering to Manning's n (Clifford et al., 1992; Parker, 1991), and an experimentally derived sediment-transport-rate coefficient (Wong and Parker, 2006). Q_w is water discharge and B is valley width. ζ is a source/sink term that could incorporate additional sediment or water supply from hillslopes or minor tributaries, an uplift/subsidence rate, and/or loss of bedload material to suspended load by gravel attrition.

4.3.2 Parametrization for the Naryn Basin

Within this model framework, we set up a fluvial network, consisting of individual, connected valley segments, where a segment's sediment and water supply is set by its upstream segments, and local base level is set by its downstream segment. We focus on the connected alluvial network upstream of the Beshkiol landslide and cut it where channels flow through bedrock segments as these are not expected to evolve significantly on our analyzed timescales and bedrock erosion not represented in the model. The derived model network includes the main trunk and all major tributaries (drainage area > 50 km^2). We measured valley width manually using the FABDEM.

The model requires inputs of water and sediment, both at the valley heads and along-stream (e.g., from hillslopes or minor tributaries not included in the tributary network). As this information is not directly

https://doi.org/10.5194/egusphere-2026-3489
Preprint. Discussion started: 14 July 2026

available, we instead estimated the values by indirect means. First, based on a global precipitation dataset (GPM IMERG Final Precipitation L3, Huffman et al., 2023) and a gauging station in the neighboring Keki catchment (Zech et al., 2021) we derived a regional yearly runoff coefficient (0.59) for that catchment. We next used that value to convert GPM precipitation in the whole Naryn catchment into local surface runoff and then computed discharge along the model network.

The boundary condition for the channel heads of the numerical model requires input Q_s and Q_w based on the following equation (Wickert & Schildgen, 2019):

$$S_0 = \left(\frac{\overline{Q_{s,0}}}{k_{Q_s}\,\overline{Q_w}}\right)^{6/7}, \tag{2}$$

with S_0 as the initial valley slope. By measuring the slope of channel heads in alluvium in the FABDEM and using the calculated $Q_{w,0}$, we can derive the sediment supply at the channel heads, $Q_{s,0}$. As discharge increases incrementally downstream in all valley segments, reflecting a continuous input of water from hillslopes and minor tributaries, we also add sediment continuously along stream, assuming a background landscape Q_s/Q_w ratio of 6×10^{-4} that we derive from averaging over all channel heads.

Two other parameters that influence the long profiles of alluvial valleys are rock-uplift rate and the downstream fining of bedload sediment (Attal & Lavé, 2009, Dingle et al., 2017; Wickert & Schildgen, 2019). Both likely impact the Naryn Basin due to its location in an actively uplifting mountain range and the presence of fine gravels in deposits beneath its terraces. As both sediment-fining and rock-uplift rates are difficult to constrain, we designed an optimization scheme to identify combinations of rock-uplift and gravel-loss rates that minimize the misfit between observed and modelled long profiles. To reduce the number of free parameters in this problem, we made the simplifying assumptions that rock uplift is spatially and temporally uniform, and that the network is equilibrated with respect to the rock-uplift rate as well as supplied water and sediment. Both assumptions are unlikely to hold in detail, but should provide sufficient first-order constraints on regional rock-uplift and gravel-loss rates to later explore how the network will respond to changes in forcing.

Additionally, we calculate the equilibration time of the network model to estimate how quickly the network adjusts to a change in external forcing or boundary condition (Paola et al., 1992; McNab et al., 2025). Paola et al. (1992) used scaling arguments and a linear diffusive framework to derive an approach for single-segment channels. McNab et al. (2025) expanded this approach to multi-branched networks resulting in the following equation:

$$T_{eq} = \frac{{k_L}^2 \langle L_I \rangle^2}{\langle \kappa \rangle}, \tag{3}$$

with equilibration time T_e, k_L as a scaling coefficient of ~1.4, L_I as mean length from all channel heads to the network outlet, and a sediment-transport diffusivity κ that defines the system's capacity to respond quicker or slower to an external change (Equation 4; McNab et al., 2023). Angled brackets indicate spatial averages over the network (McNab et al., 2025). A shorter equilibration time means that a channel or a network can adapt more quickly to an external change (e.g., in the input Q_s/Q_w ratio).

https://doi.org/10.5194/egusphere-2026-3489
Preprint. Discussion started: 14 July 2026

$$\kappa = \frac{7}{6} \frac{(k_{Q_s} I \, \overline{Q_w} \,)^{\frac{6}{7}} \, \overline{Q_{s,0}}^{\,\frac{1}{7}}}{\mathbb{S} B (1 - \lambda_p)}, \qquad (4)$$

To simulate terrace formation in the model, we track valley elevation and set a threshold value. If, after a period of aggradation, incision is deeper than the specified threshold, a fluvial terrace has formed. With further long-profile evolution, if the channel aggrades again to reoccupy the formed terrace, the terrace is removed. We therefore continuously check terrace elevation above the channel against the selected threshold value.

4.3.3 Tested Scenarios

We test the impact of climate forcing on terrace formation by changing Q_s/Q_w at all valley inlets and along stream in 23- and 41 ky sinusoidal cycles with amplitudes of 33 and 66%. We also test the effect of changing the elevation threshold for terrace formation between 2 and 5 m. In practice, we change Q_s/Q_w by changing only Q_s. Strictly speaking, Q_s and Q_w are not exactly interchangeable, because Q_w affects the efficiency of the valley response as well as its slope (Wickert and Schildgen, 2019). Nevertheless, the ratio Q_s/Q_w is the main control on long-profile evolution (Mackin 1948) and the effect of Q_w on the efficiency of the valley response can be neglected, provided variation in Q_s and Q_w is relatively small (McNab et al., 2023). At least within our modelling framework, amplitude changes of ±20% in sinusoidal variations of Q_s and Q_w have no distinguishable effects on the long profile (McNab et al., 2025). We therefore expect that varying Q_s will provide a representative view of the effects of changing Q_s/Q_w more generally, but note that minor differences may arise if Q_w varies in addition to or instead of Q_s.

We simulate river dynamics following lake drainage, using lake-bed elevation as the initial topography. Along the main Naryn River, lacustrine sediments have been mapped in detail, allowing us to construct an initial surface at the time of lake drainage (Losen et al., 2024). Based on the work of Losen et al. (2024), drainage from the first (higher) lake was rapid, possibly over the course of days, whereas the second (lower) lake drained more gradually, probably by seepage through the landslide dam. In a conservative approach, we set base-level drop for our model run to 100 yrs with an amplitude of 200 m from the downstream end of the lacustrine sediments to the base of the landslide body. Note that the lake's water level is expected to have been higher, around the upper part of the landslide body (Losen et al., 2024). Lacustrine sediments are less well preserved and/or harder to identify along the catchment's various tributaries. We therefore restrict our model to the main stream in this case. Since the main feature of the response is an upstream propagating wave of incision, we do not expect the network's configuration to play a major role, in contrast to the changing Q_s/Q_w scenario, in which signals can propagate up- and down-stream (Tofelde et al., 2019; Gioia & Schiattarella, 2020; Karssenberg & Bridge, 2008; McNab et al., 2025; Ruby et al., 2026, Savi et al., 2020; Schumm, 1973). Although simplified, this model setup allows us to test whether the observed rates of upstream signal propagation and incision of the river to its present profile are consistent with the model of Wickert and Schildgen (2019).

https://doi.org/10.5194/egusphere-2026-3489
Preprint. Discussion started: 14 July 2026

5 Results

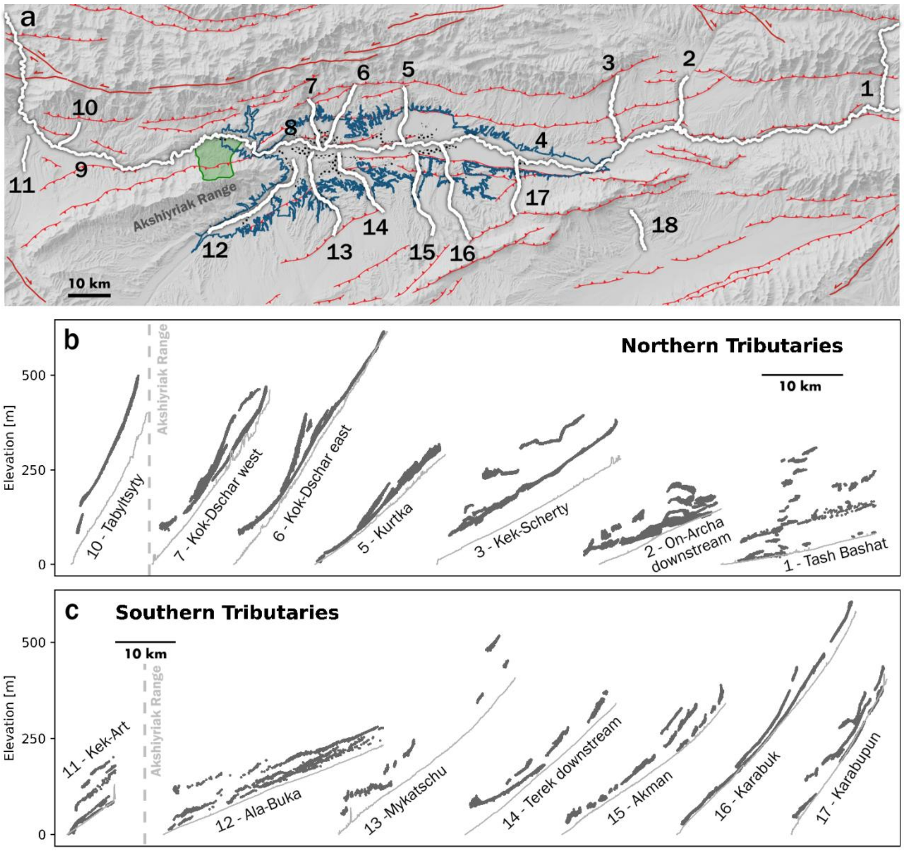

Figure 4: Tributary and terrace profiles in the Naryn Basin. (a) shows the tributary locations together with all mapped tectonic faults (AFEAD, Zelenin et al., 2022) and the lake sediments and estimated lake levels from figure 2. (b) shows tributary and terrace profiles of tributaries on the northern side of the Naryn Basin, (c) tributaries on the southern side. Note the numbering of main trunk segments that should facilitate orientation of specific sites in the Discussion section. The location At-Bashi (Site 18) is not shown in (c) as it is located in another intramountain basin separated by a bedrock gorge.

5.1 Terrace profiles around the Naryn Basin

Terrace profiles along northern and southern tributaries in the Naryn Basin show diverse characteristics (Figure 4). Several tributaries host more than one terrace generation, especially in their upstream reaches (1 – Tash Bashat, 2 – On-Archa downstream, 3 – Kek-Scherty, 7 – Kok-Dschar west, 12 – Ala-Buka, 15 – Akman, 16 – Karabupun). Some terrace profiles exhibit mostly channel-parallel slopes (1 – Tash Bashat, lower terraces of 3 – Kek-Scherty, 10 – Tabyltsyty, 12 – Ala-Buka, 16 – Karabuk, 17 – Karabupun. A few show steeper terrace slopes or even concave-up terrace profiles in the upstream sections (5 – Kurtka, 6 – Kok-Dschar east, 7 – Kok-Dschar west, 14 – Terek downstream, 15 – Akman, 16 – Karabuk). Others show lower slopes or a concave-up pattern in their downstream reaches (lower 4 km of 6 and 7 – Kok-Dschar east and west, 12 – Ala-Buka, lower 8 km of 13 – Mykatschu, lower 12 km of 14 – Terek downstream, lower 3 km of 17 – Karabupun). This pattern

https://doi.org/10.5194/egusphere-2026-3489
Preprint. Discussion started: 14 July 2026

has a spatial trend in the basin, with tributary terraces farther to the west showing higher vertical deviation from the channel and a wider lateral extent of the pattern (e.g. 12 – Ala-Buka and 13 – Mykatschu with 90 and 80 m) compared to the tributary terraces in the center of the basin or to the east. In the western and central parts of the basin, the downstream, concave-up terrace profiles tend to merge into the lacustrine sediments mapped by Losen et al. (2024) along the main stem of the Naryn River. These sediments lie at 1660 m. asl in the western basin and rise steadily to around 1700 m in the east.

5.2 Individual tributaries

In our descriptions of individual tributaries that follow, we report our new ^{10}Be derived exposure ages (table 1) and pIRIR225 depositional ages (table 2), together with any previously reported age constraints from the literature. Where ages for a given surface are widely dispersed or inconsistent with the terrace's elevation, we explain how we opt to interpret them. Later in the discussion we consider overall interpretations of the terrace chronology.

Table 1: Cosmogenic sample data table:

Sample	Latitude [°N]	Longitude [°E]	Elevation [masl]	Sample thickness (cm) / pebble count	Shielding	^{10}Be Concentration [at/g]	Error [at/g]	Age [ka]	1 sigma error [ka]
22-KG-02	41.573553	75.862733	2119	2	0.9988	222028	21066	**11.7**	**1.2**
22-KG-03	41.572792	75.861869	2117	2.5	0.9994	369966	19718	**19.0**	**1.2**
22-KG-04	41.577922	75.882514	2139	3	0.9974	502939	32354	**25.4**	**1.9**
22-KG-05	41.577422	75.882475	2141	2.5	0.9986	491572	26871	**24.7**	**1.8**
22-KG-06	41.579739	75.889867	2218	6.5	0.9993	299855	19547	**15.1**	**1.1**
22-KG-19	41.401360	73.940617	1301	3	0.9905	166286	10812	**15.8**	**1.2**
22-KG-20	41.401305	73.940627	1301	2	0.9905	118479	7593	**11.4**	**0.8**
22-KG-21	41.397830	73.940106	1309	2.5-3	0.9921	68598	7378	**6.8**	**0.7**
22-KG-22	41.395695	73.939631	1314	3	0.9877	77372	7295	**7.6**	**0.7**
22-KG-30	41.127490	74.983030	2382	2	0.9985	357051	23428	**15.7**	**1.1**
22-KG-31	41.127460	74.982790	2382	2	0.9983	494411	23879	**21.2**	**1.3**
22-KG-32	41.127310	74.982090	2382	3	0.9982	321930	23771	**14.4**	**1.2**
22-KG-33	41.104285	74.975419	2559	102 pebbles	0.9986	4710932	180800	**183.5**	**10.5**
22-KG-34	41.104220	74.975055	2558	2.5	0.9986	226983	20195	**9.3**	**0.9**
22-KG-35	41.100501	74.985301	2434	113 pebbles	0.9928	194591	15862	**8.7**	**0.8**
22-KG-36	41.159834	74.984238	2262	107 pebbles	0.9987	161802	14845	**8.0**	**0.8**
22-KG-39	41.498263	76.429625	2292	3	0.9959	86093	15579	**4.6**	**0.8**
22-KG-41	41.543299	76.460383	2429	3.5-4	0.9964	161691	17743	**7.4**	**0.8**
22-KG-42	41.543525	76.460174	2429	3.5	0.9964	209910	15521	**9.3**	**0.8**
22-KG-43	41.543855	76.458587	2427	3	0.9974	225884	17149	**10.0**	**0.8**
22-KG-44	41.498284	76.429793	2293	3	0.9959	359359	20662	**16.7**	**1.1**
22-KG-49	41.438188	75.337624	1861	121 pebbles	0.9991	2218680	90544	**134.6**	**8.4**

https://doi.org/10.5194/egusphere-2026-3489
Preprint. Discussion started: 14 July 2026

22-KG-50	41.497519	76.406581	2278	2	0.9967	337372	21358	**15.8**	**1.1**
22-KG-51	41.497741	76.402318	2272	2	0.9961	177952	16356	**8.7**	**0.8**
22-KG-52	41.505940	76.411226	2430	2.5-3	0.9983	867349	36286	**35.8**	**2.1**
22-KG-53	41.506910	76.413318	2434	3	0.9983	1620129	57340	**67.0**	**3.8**
22-KG-54	41.506119	76.411308	2430	4	0.9983	481627	23419	**20.2**	**1.3**
22-KG-55	41.510352	76.418921	2488	4-4.5	0.9984	125679	24478	**5.7**	**1.0**
22-KG-56	41.510418	76.418835	2487	3.5	0.9984	1351608	60977	**54.4**	**3.6**
22-KG-58	41.509640	76.416683	2483	3.5	0.9983	669662	28314	**26.9**	**1.6**
22-KG-59	41.599691	75.911106	2293	2	0.9981	312651	19259	**14.5**	**1.0**
22-KG-60	41.599694	75.912799	2308	2	0.9974	2289390	108641	**102.6**	**6.3**
22-KG-61	41.603607	75.910866	2282	1	0.9987	116756	15051	**5.9**	**0.7**
22-KG-64	41.610476	75.901087	2295	2.5	0.9991	705562	31874	**31.7**	**2.1**
22-KG-65	41.610412	75.901227	2295	2.5	0.9991	171040	16700	**8.26**	**0.8**
22-KG-66	41.610648	75.901454	2295	3	0.9991	443429	25244	**20.2**	**1.4**

Table 2: Luminescence sample data table:

Sample	**Latitude [°N]**	**Longitude [°E]**	**Depth [m]**	**Dose rate [Gy/ka]**	**Water content [%]**	**Equivalent dose [Gy]**	**N° of aliquots**	**pIRIR225 age [ka]**	**1 Sigma error [ka]**
22-KG-08	41.425125	74.738692	2.27	3.66 ± 0.23	15 ± 5	71.82 ± 13.47	20	**19.63**	**3.89**
22-KG-13	41.414801	74.078913	0.7	3.63 ± 0.23	15 ± 5	69.02 ± 8.44	19	**19.01**	**2.62**
22-KG-15	41.398345	74.017483	2.5	3.67 ± 0.23	15 ± 5	305.33 ± 23.98	19	**83.17**	**8.41**
22-KG-17	41.383230	74.947290	4.0	6.01 ± 0.34	15 ± 5	649.87 ± 54.13	15	**108.11**	**10.86**
22-KG-23	41.423050	74.745660	0.85	3.90 ± 0.24	15 ± 5	75.63 ± 6.92	24	**19.38**	**2.13**
22-KG-27	41.413960	74.777100	1.3	3.60 ± 0.23	15 ± 5	99.44 ± 13.54	24	**27.59**	**4.16**
22-KG-37	41.392028	75.661683	2.3	3.77 ± 0.23	15 ± 5	113.09 ± 15.81	24	**30.01**	**4.59**
22-KG-38	41.392641	75.660106	5.7	3.94 ± 0.24	15 ± 5	219.43 ± 33.40	24	**55.73**	**9.15**
22-KG-40	41.503665	76.433669	1.7	4.16 ± 0.25	15 ± 5	95.62 ± 10.56	21	**23.02**	**2.89**
22-KG-45	41.209736	75.730154	3.7	3.52 ± 0.23	15 ± 5	53.30 ± 7.16	22	**15.13**	**2.27**

https://doi.org/10.5194/egusphere-2026-3489
Preprint. Discussion started: 14 July 2026

Tash Bashat (Site 1):

The location hosts several terrace levels (Figure 5a, b) that we sampled for surface exposure dating, while we took an additional luminescence sample 1.7 m below the surface of the most widespread level, located 68 m above the modern channel. The two highest surfaces reveal substantial scatter in sample exposure ages (from ca. 6 to 67 ka), complicating interpretations of the timing of terrace abandonment. The luminescence sample, from an intermediate terrace level with an age of 23.0 ± 2.9 ka, sits in fine-grained sediment that we interpret as a mixture of loess, overbank deposition and, probably, colluvium due to the inclusion of rare, small pebbles within this unit. This age is only moderately older than two exposure ages from the same surface (15.8 ± 1.1 ka, 16.7 ± 1.1 ka), whereas two other samples yield substantially younger exposure ages (8.7 ± 0.8 ka, 4.6 ± 0.8 ka).

In other parts of the Naryn Basin, we observed cobble and boulder groupings, likely accumulated by human activity. We therefore explain the relatively young sample ages of these surfaces with exhumation, turnover or rolling. We reject the possibility of significant inheritance to the ^{10}Be concentration, as younger ages for these surfaces would imply incision or uplift rates nearly an order of magnitude higher than reported for faults in the region (Thompson et al., 2002; Goode et al., 2014), giving the older sample ages a higher likelihood to represent the actual terrace abandonment age. We therefore interpret terrace abandonment of the most widespread level, 68 m above the channel, to have occurred between the pIRIR225 age of 23.0 ± 2.9 and ^{10}Be age of 15.8 ± 1.1 ka. This interpretation requires rejection of the samples with exposure ages between 10.0 ± 0.8 and 7.4 ± 0.8 ka one level above, at 160 m above the channel, despite the fact they cluster well.

On-Archa upstream (upstream of Site 2):

This site hosts one terrace ~12 m and two higher surfaces ~50 and 110 m above the current channel (Figure 5 c, d); limited exposure of the highest one makes it difficult to correlate along stream. In the upper reach, this surface splits into two levels, representing potential impacts of two tributary confluences at the same location. Furthermore, south-east of the channel, the same surface slopes towards the channel, eventually accounting for a large vertical elevation scatter (110-150 m above the channel).

The area is cut by at least one fault that crosses the tributary downstream with an east-west strike. We interpret the lower surface to have an age between 19 and 25 ka and the large scatter in exposure ages of the high surface to result from a combination of shielding or turnover of the cobbles and boulders. We estimate the high terrace to be > 30 ka, with a small likelihood of being significantly older (~100 ka). A terrace patch 9 km downstream of the location, situated at 2100 m elevation, or 80 m above the channel, has a minimum age of 143 ± 15 and 150 ± 23 ka dated by thermoluminescence and IRSL (Thompson et al. 2002).

Kek-Scherty (Site 3):

At this site, a prominent fault cuts two terrace levels (Figure 5e, f). By dating the lower surface with ^{14}C between ~13 and 15 ka, Thompson et al. (2002) derived a fault slip rate of 1.5 ± 0.3/0.4 mm/yr. As well as the large offset over the fault, the higher terrace shows a depression upstream, possibly associated with a local down-drop structure.

At-Bashi (Site 18):

The study site reveals three major terrace levels at ~20, ~50 and 120 m above the channel, the lowest of which is split into three sub-levels (Figure 5g, h). Perpendicular to the flow direction, terrace surfaces slope towards the

https://doi.org/10.5194/egusphere-2026-3489
Preprint. Discussion started: 14 July 2026

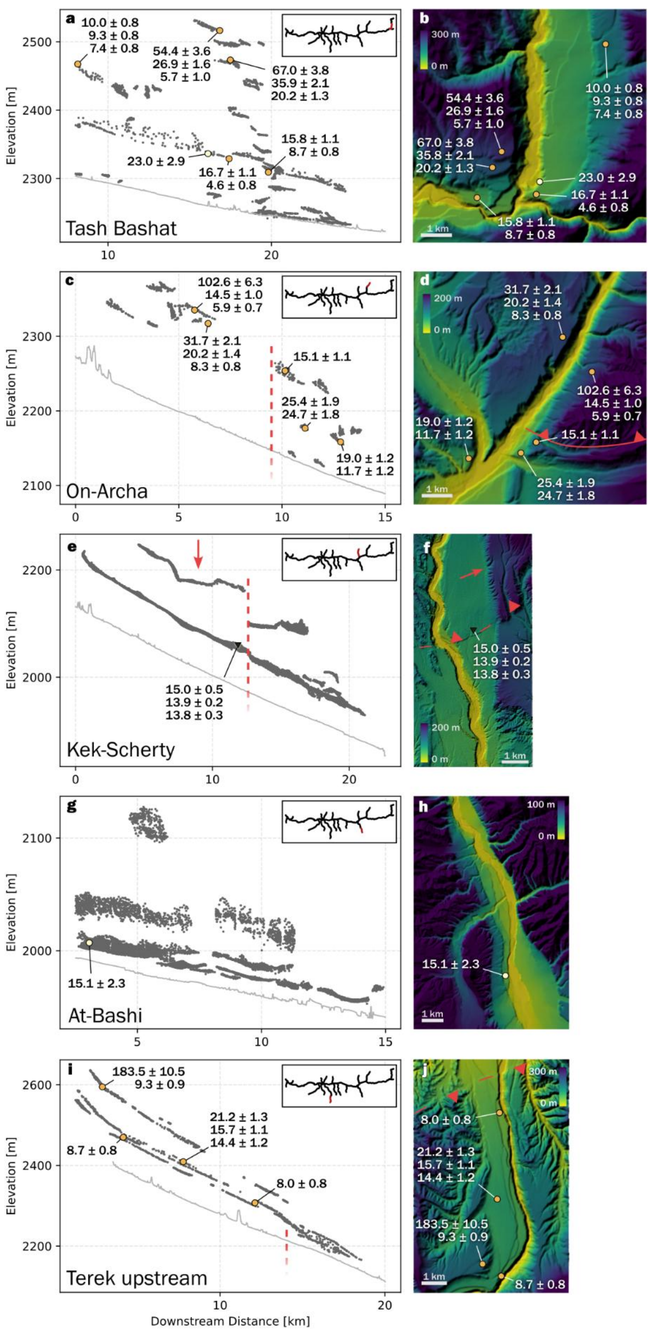

Figure 5: Tributary channel and terrace profiles in selected locations. (a), (c), (e), (g) and (i) show in dark grey dots terrace elevations and in a thin grey line the channel elevation. (b), (d), (f), (h) and (j) show DEMs colored by relative elevation above the channel. Bright yellow points: luminescence samples; orange circles: Cosmogenic nuclide samples. Red lines show faults from the AFEAD database. Red line in (f) and (j) is dashed for better fault visibility. Red arrows in (e) and (f) indicate the surface depression mentioned in the text. Vertical elevation scatter in modern river long-profiles result from resolution artefacts of narrow channels and valleys in 30 m pixels.

river and are dissected by rills and channel depressions resulting in a higher vertical spread in terrace elevation. One luminescence sample from fine-grained sediment (interpreted to be a mixture of aeolian, overbank and loess deposits) topping fluvial gravels within the lowest terrace yields an pIRIR225 age of 15.1 ± 2.3 ka, providing a minimum age constraint on the underlying terrace gravels.

https://doi.org/10.5194/egusphere-2026-3489
Preprint. Discussion started: 14 July 2026

Terek upstream (upstream of site 14):

The site hosts three terrace levels that occur south of a northward verging blind thrust (Figure 5i, j). The middle terrace is the most widespread and spans nearly the full valley width. All three surfaces are slightly steeper than the recent channel, with higher slopes on the highest surface.

As the lower two surfaces yield exposure ages that are well clustered and stratigraphically consistent (ca. 15 to 21 ka), we disregard the younger age of 9.3 ± 0.9 ka on the highest surface, and instead prefer the age of 183.5 ± 10.5 ka. The lower surface yielded two exposure ages that agree within uncertainty (8.7 ± 0.8 and 8.0 ± 0.8 ka).

Naryn Central (Site 4):

The site reveals one very high alluvial surface (~178 m above the modern channel), one lower widespread level (between 30 to 45 m above the modern channel), and several higher and lower elevation patches that cannot be straightforwardly classified into distinct terrace generations (Figure 6c, d). Within the widespread terrace level, two samples from the same fine-sand stratigraphic unit at depths of 5.7 and 2.3 m yielded pIRIR225 ages of 55.7 ± 9.2 and 30.0 ± 4.6 ka, respectively. We interpret the terrace abandonment to be younger than the depositional age of 30 ky.

Kok-Dschar east (Site 6):

About 2.5 km east of the channel (Figure 4b, channel number 6), Goode et al. (2014) reported a minimum OSL derived terrace age of 270 ± 17 ka for a low and continuous terrace.

Kok-Dschar west (Site 7):

Goode et al. (2014) reported ^{14}C ages of 14.0 ± 1.0 and 6.1 ± 0.1 ka from a lower elevation patch and 13.0 ± 1 ka from a higher patch at this location (Figure 4b, channel number 7). They hypothesized one thick aggradational body represented by the samples of 14 and 13 ka, whereas the 6-ka age might indicate a younger, smaller inset fill terrace.

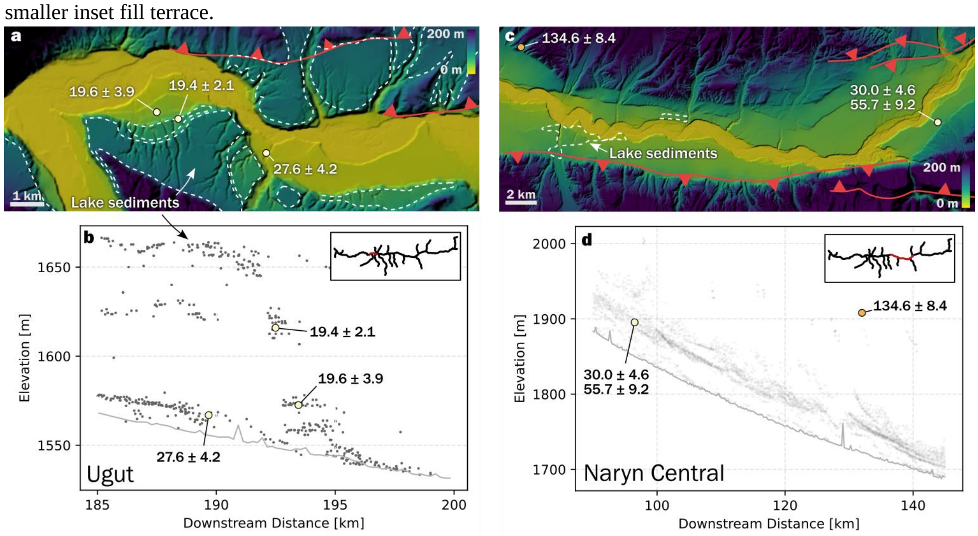

Figure 6: Trunk channel and terrace profiles in selected locations. (a) and (c) show DEMs colored by relative elevation above the channel. Red lines show faults from the AFEAD database. (b) and (d) show in dark grey dots terrace elevations and in a thin grey line the channel elevation. Available sample are shown with their calculated age. The color of the sample points refers to the dating method shown in figure 1.

Ugut (Site 8):

This site, which is situated downstream from the "Naryn Central" site, hosts four surfaces, with at least the upper two covered by lake sediments according to Losen et al. (2024) (Figure 6a, b). One luminescence sample collected 0.85 m below the 2nd highest surface gives an pIRIR225 age of 19.4 ± 2.1 ka. From the next surface below, a sample collected 2.27 m below the surface, and 45 m below the previous sample, yields an age of 19.6 ± 3.9 ka.

The ages and sedimentary appearance of both samples (upper sample collected from loose, laminated, silty material; the lower sample comprising mostly silt and clay) suggest they are part of the Erkin Formation described by Losen et al. (2024). Additionally, their similar age despite their elevation difference of 45 m could indicate that lacustrine sediments here cover a preexisting terrace sequence. A third luminescence sample from the lowest terrace surface yielded an pIRIR225 age of 27.6 ± 4.2 ka. We interpret the sediments from the first two samples as having been deposited during the presence of the lake, whereas the fine-grained sediment around the third sample probably reflects locally restricted water flow during earlier fluvial deposition.

Kazarman (Site 9):

The site, on the main Naryn channel west of the bedrock gorge in the Akshiyriak Range and therefore downstream of the Beshkiol landslide (Figure 7a, b), hosts four surfaces, with the two intermediate surfaces being the most widespread. The 2nd highest surface consists of interfingering layers of gravels and sand-silt lenses, and a luminescence sample collected 2.5 m below the surface yielded a pIRIR225 age of 83.2 ± 8.4 ka. The terrace level below yielded an pIRIR225 age of 19.0 ± 2.6 ka from fine-grained material incorporating rare pebbles and cobbles sampled 0.7 m below the surface.

Directly below the ca. 19 ka luminescence sample, we sampled a thick layer of fluvial gravels for a cosmogenic ^{10}Be depth profile (Figure 7c, d). Scatter in the depth profile of ^{10}Be concentrations results in a poor fit to the expected exponential function and does not allow a straightforward exposure age calculation. Nevertheless, if we assume instantaneous deposition of fine-grained sediments above the gravels at 19.0 ± 2.6 ka (as indicated by the pIRIR225 age), the predicted distribution of ^{10}Be concentrations with depth is broadly consistent with the measured concentrations, though a statistically better fit is possible (Figure S2). Given the uncertainty, we conclude that the ^{10}Be depth profile does not contradict the interpretation of the 19.0 ± 2.6 ka pIRIR225 age as constraining the end of sediment deposition, and therefore closely approximating the timing of terrace abandonment. See Supplementary figure S2 for further discussion of the profile.

Tabyltsyty (Site 10):

The site consists of a main terrace level 110 m above and sub-parallel to the current channel, and a smaller inset terrace patch with a steeper slope that occurs immediately before the confluence with the main Naryn channel (Figure 4a, b, channel number 10).

https://doi.org/10.5194/egusphere-2026-3489
Preprint. Discussion started: 14 July 2026

Kek-Art (Site 11):

The site hosts 5 terrace levels (Figure 7e, f), with the 2nd highest yielding a luminescence age of 108.1 ± 10.9 ka 4.0 m below the surface where gravel and sand layers interfinger. West of this sample location, a bedrock ridge confines the channel into a narrow canyon (vertical elevation data spread in Figure 7e). A lower terrace level yielded four poorly clustered exposure ages that range from 6.8 ± 0.7 ka to 15.8 ± 1.2 ka.

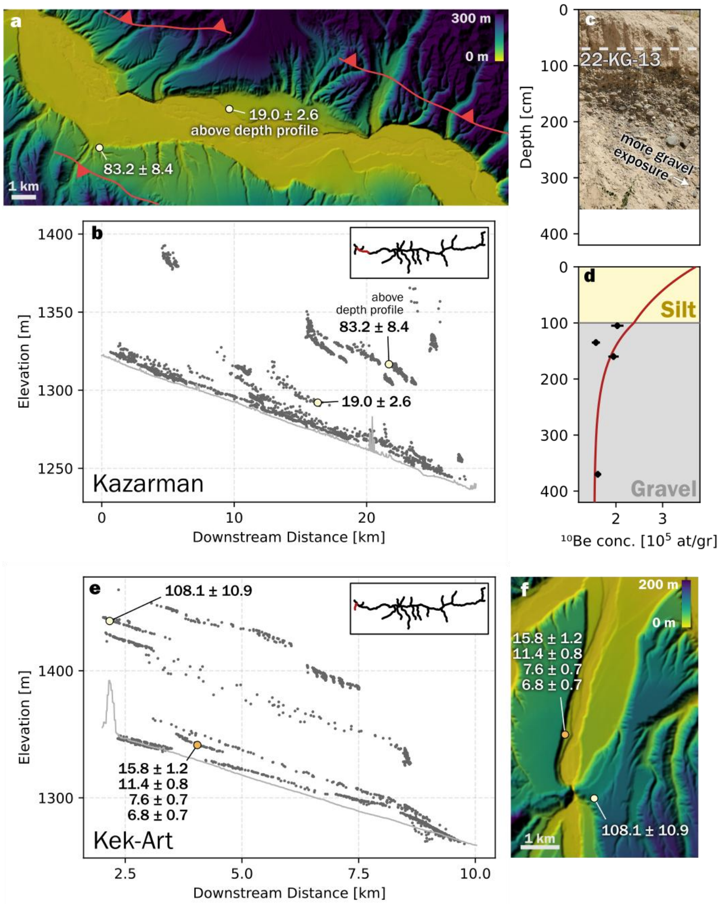

Figure 7: Channel and terrace profiles in selected locations together with a ^{10}Be depth profile. (a) and (f) show DEMs colored by relative elevation above the channel. Red lines show faults from the AFEAD database. (b) and (e) show in dark grey dots terrace elevations and in a thin grey line the channel elevation. Dated samples are shown with their calculated ages. The color of the sample points refers to the dating method shown in figure 1. (c) shows a field photograph together with the depth the sample 22-KG-13, indicated with the dashed white line (0.7 m; pIRIR225 age of 19.0 ± 2.6 ky). (d) shows the ^{10}Be concentration (red line) for 19.0 ± 2.6 ky of exposure for a profile consisting of 1 m silt with rare pebbles overlying > 3 m of gravel. Black points show ^{10}Be concentrations of amalgamated pebble samples.

5.3 Terrace modelling

5.3.1 Network implementation

We first present results of our optimization approach to estimate rock-uplift and gravel-loss rates for the Naryn Basin alluvial network, shown in Figure 8a. The lowest misfit value of 80.5 m (6.8 % of original DEM network relief, Figure 8c) is achieved with the parameter combination of 0 mm/yr uplift and 2.4 % gravel loss per kilometer (white cross in Figure 8b). Nonetheless, an approximately linear trade-off is apparent such that similarly low misfits are possible for nonzero uplift rates, provided they are balanced by increasing gravel loss. Based on all points below a RMSE threshold of 100 m, we derived a linear regression describing this balance between gravel loss l_{gravel} (fractional loss per kilometer) and the uplift rate $\dot{U}$:

https://doi.org/10.5194/egusphere-2026-3489
Preprint. Discussion started: 14 July 2026

$$l_{gravel} = 0.85\dot{U} + 2.41 \quad (5)$$

Based on age and elevation offsets between individual terrace levels in the Naryn Basin, we derive a mean incision rate of 1 mm/yr (between 0.3 and 2.8 mm/yr) corresponding to a gravel loss rate of 3.3 %/km. This value lies within the range derived by Attal & Lavé (2009) in experimental studies for a range of lithologies, including limestone, granite and sandstone, which are the main rocks cropping out in our field area. The remaining discrepancies between the original network elevation and the starting network model (Figure 8c) could be attributed to localized fault activity (Thompson et al., 2002; Goode et al., 2014), disequilibrium within the network, variations in the fixed channel-head drainage-area threshold (Clubb et al., 2014), or deviations from our assumed constant along-stream sediment supply.

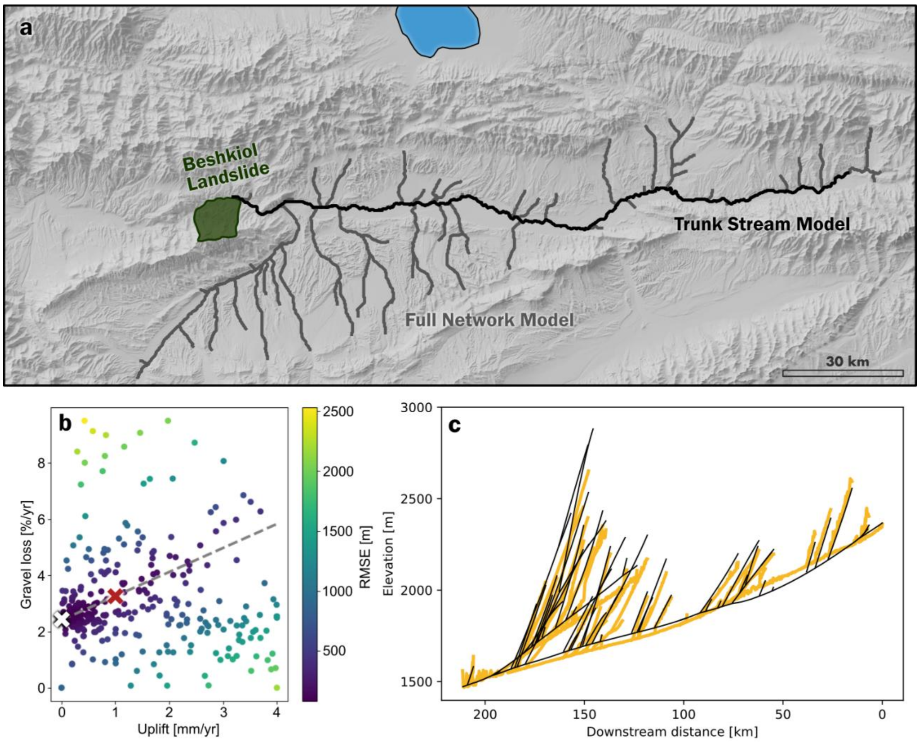

Figure 8: (a) shows the drainage channels incorporated into either the full network model or the trunk-stream-only model. (b) shows the misfit space of the model parametrization for downstream gravel loss and rock uplift. White cross marks the algorithms lowest misfit, whereas the grey dashed line marks the line of lowest misfit and the red cross marks the parameter combination we used, 1 mm/yr uplift and 3.3 % gravel loss per kilometer. (c) shows the original network elevation derived from the DEM in yellow and the model starting elevation derived based on values from (b) in thinner black lines

To estimate the network equilibration time, following the definition of McNab et al. (2025), we calculated a mean inlet length of 96.2 km and a mean diffusivity of 1.0476 x 10^{-3} m^2 s^{-1}, resulting in an equilibration time of 550 ky. This result implies that orbital climate cycles, and the filling and draining of the Beshkiol landslide lake, occurred on timescales much shorter than that over which the fluvial network can equilibrate. We would

https://doi.org/10.5194/egusphere-2026-3489
Preprint. Discussion started: 14 July 2026

495 therefore expect aggradation and incision associated with these drivers, and potentially recorded in fluvial terraces, to be transient and incomplete.

5.3.2 Terrace Formation from Cyclic Climate Forcing

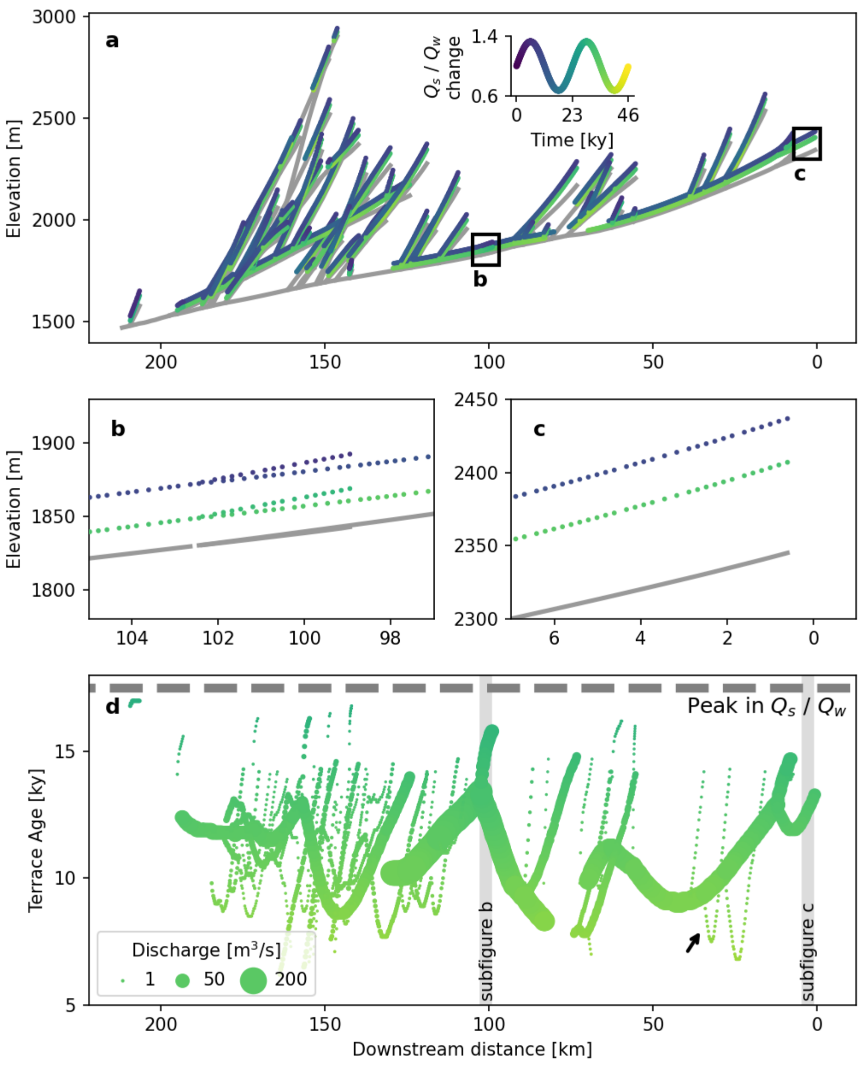

Figure 9: Numerical modelling results in response to sinusoidal change in the sediment-to-water ratio Q_s/Q_w. (a) shows terrace formation across the network. (b) and (c) show two different in-detail parts of the network, marked with black rectangles in (a). (d) shows the spread of terrace formation age of the younger and lower terrace generation of the two modelled ones in (a), (b) and (c). Note that points represent terrace segments along stream with point size scaled to respective channel discharge and color representing terrace abandonment age. Locations of both subfigures (b) and (c) are shown with grey vertical bars. Thick horizontal dashed line represents peak in Q_s/Q_w at 17.25 ky before the model stops. See supplement figure S 1.4 for a brief exploration of the dependency between the amplitude of Q_s/Q_w change, periodicity of the input signal and the terrace detection threshold.

https://doi.org/10.5194/egusphere-2026-3489
Preprint. Discussion started: 14 July 2026

We forced the network model by sinusoidally varying the Q_s/Q_w ratios of each valley inlet and the along-stream sediment supply with different amplitudes (± 33 % and 66% of their mean values) and orbital periodicities (23 and 41 ky), and implemented two terrace formation and preservation thresholds (2 and 5 m). Here, we show the results for the combination of a ± 33 % change in upstream and along-stream sediment supply in 23-ky cycles with a terrace-formation and -preservation threshold of 2 m (Figure 9). An increase in the sediment-to-water supply ratio at the valley inlets induces a downstream-propagating aggradation signal. When Q_s/Q_w reaches a maximum and then begins to decrease, a wave of incision initiates at valley heads and also propagates downstream, forming a terrace (Figure 9c). However, even with continuous forcing cycles, terraces do not extend throughout the valley network. Rather, they are restricted to lower order tributaries close to valley inlets and parts of the main trunk stream. In particular, terraces are absent from the downstream sections of the main trunk stream and some of the longer tributaries. This pattern reflects the difference between the implemented forcing periodicity and the network-equilibration time of 550 ky, leaving the network only a fraction of the time needed to adjust to the changing external conditions. Thus, among all tested parameters (signal periodicity, Q_s/Q_w amplitude change, and terrace detection threshold), the periodicity of the input signal exerts the strongest impact on terrace formation, particularly on its downstream extent (Supplement figure S 1.4).

The model predicts that terrace formation will occur diachronously throughout the network, with predicted ages for the youngest terrace generation ranging from 17 to 6 ky prior to the end of the model (Figure 9d). These ages correspond to terrace-formation lag times of c. 0 to 11 ky relative to the peak in Q_s/Q_w at 17.25 ky prior to the end of the model, or up to about one half of the forcing period. Patterns in the timing of terrace formation reflect the propagation of signals through the network (see McNab et al., 2025, for a general discussion). Increasing terrace-formation ages with distance downstream reflect downstream signal propagation, while decreasing ages reflect upstream propagation. Steeper lines in terrace age—downstream distance space represent slower signal propagation, while gentler lines represent faster propagation.

Signal is introduced at the valley inlets and propagates downstream, resulting in terrace ages that increase downstream away from the inlets. This dynamic is similar to that shown for a single-segment river by Ruby et al. (2026; see their Supplementary Material for an animation). Note that two kinds of inlet segment are present in our model. First, we include lower order streams, with drainage areas close to our threshold of 50 km^2, with which we aim to capture approximately the first transition from bedrock to alluvial dynamics (small points in Figure 9d). Second, we include larger tributaries that cross bedrock gorges before entering our specific alluvial sub-basin (larger points in Figure 9d). The latter have larger discharges, so that signals can propagated more quickly along them. Furthermore, segment length varies throughout the domain. Therefore, higher order segments receive signal from upstream inlets at different times, as well as directly due to varying along-stream sediment supply. Since aggradation and incision on higher order segments varies the local base level of upstream segments, these patterns can result in signal from shorter, higher discharge inlet segments being propagated back upstream via higher order segments.

Various examples of these dynamics are visible in Figure 9d. Along the main trunk stream, terraces are oldest (i.e., lag times are shortest), at confluences with major, but short tributaries (e.g., Figure 9d, location of subfigure b). These points form peaks in terrace age—downstream distance space, from which signal propagates both up- and down-stream. Meanwhile, on longer, lower order tributaries, signal propagating upstream can dominate close to their confluences with higher order segments. As such, moving away from their inlets, terrace ages first increase slowly, before reaching a minimum and beginning to decrease towards the confluence (Figure 9d, arrow). The youngest terraces in the network (i.e., the longest lag times), are found at these minima.

5.3.3 Terrace Formation from Lake Drainage

Modelling a single episode of base-level fall associated with lake drainage results in an upstream migrating incision wave with a knickpoint that is progressively smoothed out upstream into a broader convexity or knickzone (Figure 10), and an upstream migration rate that decreases with time. Associated abandonment of the terrace surface (which in this case is the upper surface of the lake sediments) follows this upstream propagating wave of incision. The age of terrace formation decreases from 20 ka at the downstream end, corresponding to the onset of base-level drop, to 8.9 ka at the upstream end. The resulting terrace profile closely resembles the initial lake sediment elevation, with a concave-up pattern. After 20 ky of model run-time, the channel profile did not yet reach its long-term equilibrium, again highlighting the difference between the 20 ky runtime of the model run and the network's equilibration time of 550 ky.

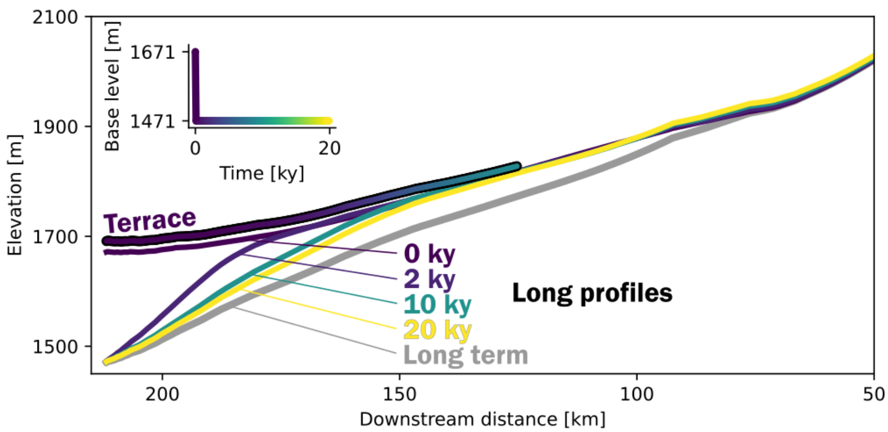

Figure 10: Modelled fluvial response to sudden base-level drop with formed terrace and valley long profiles of different timesteps, labelled accordingly. Note that only a portion of the trunk stream is shown to better visualize the modelling results.

https://doi.org/10.5194/egusphere-2026-3489
Preprint. Discussion started: 14 July 2026

6 Discussion

6.1 Geochronology

From both our dating results (despite their overall dispersion) and those from the existing literature, we can identify some common periods of terrace abandonment. These occur at around 180 ka, between 120 and 150 ka, around 80 ka, and most clearly throughout the region, between 15 and 20 ka (Figure 11b). Surfaces of the latter range of ages cluster often form a continuous and widespread terrace within their site-specific sequence. This time window also includes a minimum in northern hemisphere summer insolation (Figure 11a, Laskar et al., 2004), as well as a $\delta^{18}O$ maximum in the Kesang Cave record that inversely correlates with Central Asian temperature (Figure 11b, Cheng et al., 2012). However, during that same time period, the large paleolake occupied the Naryn Basin, draining catastrophically at around 15 ka (Losen et al., 2024), providing an alternative, coeval mechanism for terrace formation. From a geochronological perspective alone, disentangling the two signals is therefore not possible. We consider next how terrace profiles and the insights gained from terrace modelling might enable us to disentangle the different terrace formation mechanisms.

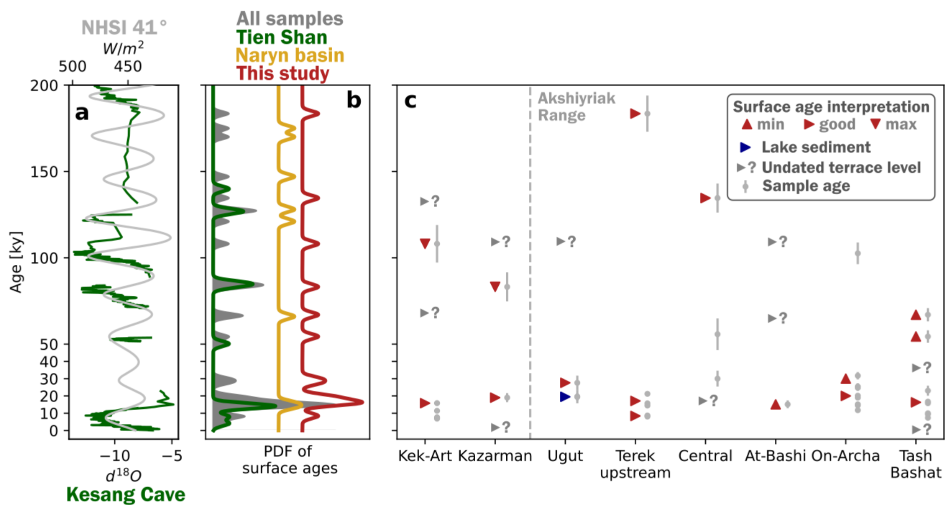

Figure 11: Summary figure of terrace chronology and sequences. (a) Kesang cave data and northern hemisphere summer insolation at 41° for context. (b) probability density function of different sample groups: studies in the whole Tien Shan (green, Thompson et al., 2002; Campbell et al., 2019; Selander et al., 2012; Cording et al., 2014), in the Naryn Basin (yellow, Thompson et al., 2002; Goode et al., 2014; Losen et al., 2024), this study (red, excluding the lake sediment samples at Ugut) and all samples together (grey in the background). (c) each study sites' sample ages (grey points) and interpreted surface ages (red triangles). Grey triangles with question mark are non-dated surfaces.

6.2 Terrace profile shapes and spatial distribution

The shape and spatial extent of tributary terrace profiles reflect the mechanisms that formed them. Here we consider the possible roles of tectonic activity, base-level fall during lake drainage, and climatic variations in generating the terrace record.

https://doi.org/10.5194/egusphere-2026-3489
Preprint. Discussion started: 14 July 2026

Faults in the Naryn basin strike mostly east–west, crossing tributary channels and deforming terraces over length scales of up to a few kilometers (e.g. 2 – On-Archa, 3 – Kek-Scherty, 7 – Kok-Dschar west in Figure 4). While this type of localized fault deformation of terraces is readily apparent, whether fault activity could have affected the whole network is unclear. Based on the geologic setting, with the Naryn River flowing westward along an intermontane basin before crossing northward through the Moldo-Too Range (Figure 1), it is possible that a change in activity along the faults bounding the Moldo-Too Range could affect the whole Naryn river network, i.e., by inducing a change in the base-level fall rate at the outlet. However, most terraces along tributaries that are unaffected by localized faulting, particularly those in the upper reaches of the tributaries, are either sub-parallel to or steeper than the modern channel. This geometry argues against channel incision and terrace formation being induced by a regional increase in rock-uplift rates or base-level fall rates (see Section 3b).

Exceptions to this argument are found in the lower reaches of tributaries up to ca. 60 km upstream from the Beshkiol landslide, where terraces are concave-upward and less steep compared to the modern channel profiles (Figure 4). If these terraces were formed as a result of changes in activity along the faults bounding the Moldo-Too Range, we would expect to see similarly divergent terraces along the lower reaches of tributaries downstream of the Beshkiol landslide, but we do not (see channels 10 -Tabyltsyty and 11 - Kek-Art, Figure 4). The spatial pattern of divergent terraces is instead consistent with parts of our conceptual model in Figure 3c, in which lacustrine hemipelagic sedimentation, in this case upstream from the Beshkiol landslide, forms such terrace shapes. This interpretation is further supported by the mapping of the predominantly muddy, lacustrine Erkin and Sultan Formations. However, we observe no obvious breaks in terrace slopes that might be indicative of fan deltas with transitions from topsets to foresets (Figure 3c); this could reflect finer grain sizes on average transported by the tributaries during that period, varying lake levels, or poor preservation potential of the coarser-grained deposits.

Although the terrace profiles at the Tabyltsyty and Kek-Art sites, downstream of the Beshkiol landslide, should not have been impacted by any lake sedimentation, they still yield terrace-formation ages between 15 and 20 ka (Figure 7 and 11), suggesting climate played a role in terrace formation at these locations. We consider this point further below.

6.3 Insights from Terrace Modelling

The modelled fluvio-lacustrine terraces in the lake-drainage scenario fit the tributary terraces in their concave-up shape as well as, to a first order, in their spatial extent and time lag of formation. The model overpredicts the distance upstream the channel-incision signal has propagated: in the model, it reaches about 90 km upstream, between the Karabupun and Kek-Scherty sites (Figure 10), compared to the observed extent around 53 km upstream, between the Kurtka and Akman sites (Figure 4). This discrepancy could result from moderate differences between actual and modelled network properties such as water discharge and valley width. Lower discharges or wider valleys during the incision phase could potentially have slowed down terrace formation. The available geochronology from the Naryn Basin, including our and previously published results, is too imprecise to resolve these lag times in terrace formation.

However, the mechanism of lake-drainage cannot explain terraces formed in the upstream reaches of the tributary network or downstream of the Beshkiol landslide (e.g., Terek upstream in Figure 5, 1 – Tash Bashat or 10 – Tabyltsyty in Figure 4) or the formation of several surfaces in one location (Figure 4-7). In contrast, the numerical modelling results for the climate-induced scenario do predict terrace formation of multiple generations across the upstream reaches of tributaries throughout the study area and, in places, along the main trunk stream. This result is somewhat unexpected, as previous work modelling a single-treaded channel highlighted limited downstream signal propagation in systems with similar or even lower ratios of forcing periodicity to the system's equilibration time (Ruby et al., 2026). Results here emphasize the potential importance of signal propagation within river networks, as even the shorter of the two tested periodicities (23 ky and 41 ky) produces terrace extents that reach the trunk stream and therefore spatially overlap with terraces associated with lake drainage.

Furthermore, modelled heights and slopes of climate change induced terraces are consistent with observed terrace profiles throughout the Naryn basin. Modelled upstream reaches show terrace heights of > 50 m and steeper slopes than the modern channel (Figure 9c), matching observations at several sites (3 – Kek-Scherty, 15 – Akman, 16 – Karabuk, 17 – Karabupun in Figure 4c; Tash Bashat and On-Archa downstream in Figure 5a and c). In contrast, modelled downstream reaches host sub-parallel terraces of ~20 m (Figure 9b), similar to observed elevations and slopes patterns at several downstream sites (e.g. Naryn central, At-Bashi, Kek-Art and Kazarman).

6.4 Interpretation of the terrace record

We interpret that lake-drainage mainly impacted the lower reaches of the main Naryn trunk and its tributaries in the western part of the basin, whereas Q_s/Q_w change best explains terrace formation in the upstream tributary reaches and downstream of the Beshkiol landslide. Nevertheless, discrepancies between our climate-model predictions and observations remain. The model predicts, for example, more gently sloped terraces at lower relative elevation than observed at the Terek site (Figure 5i). These site-specific differences could be minimized with a stronger Q_s/Q_w amplitude change, higher uplift in response to the nearby blind thrust, or with a longer climate periodicity, showing the potential of including alluvial long-profile modelling when inferring paleoclimatic signals from terrace sequences at specific study sites.

By identifying climate changes as a regional driver of terrace formation, we can link the climate-induced terrace record to paleoclimate archives and the broader context of landscape change during the LGM. Beside speleothem trace elements and $\delta^{13}C$ in the Kesang Cave that indicate wetter glacial environments (Cheng et al., 2016), most previous work considered the LGM to have been relatively dry based on loess profiles (Fitzsimmons et al., 2018; Youn et al., 2014; Song et al., 2018; Li et al., 2018; Kang et al., 2015), pollen records (Grigina & Fortuna, 1981) and limited stalagmite growth in the Kesang Cave (Cheng et al., 2012; Cheng et al., 2016). Zhang et al. (2023), in contrast, correlate terrace abandonment to peak glacial conditions, which they interpreted to reflect a high-discharge setting and hypothesized limited evaporation during the LGM as the driving force. The decrease in Q_s/Q_w that we infer during the LGM or immediately following peak glacial conditions could result from either decreased sediment flux (Q_s) or increased water discharge (Q_w). While decreased loess availability and deposition (Fitzsimmons et al., 2018; Youn et al., 2014; Song et al., 2018; Li et

https://doi.org/10.5194/egusphere-2026-3489
Preprint. Discussion started: 14 July 2026

al., 2018; Kang et al., 2015) and (tree-) vegetation re-establishment on the hillslopes (Grigina & Fortuna, 1981) probably indicate substantially reduced Q_s, these processes could also be caused by higher precipitation that increased Q_w. Thus, without tighter constraints on Q_s or Q_w, we cannot resolve the details of their change. Nevertheless, the systematic Q_s/Q_w decrease recorded in fluvial terraces in the Naryn basin documents how global glacial-to-interglacial climate changes altered landscape processes and how those changes were ultimately transferred to the fluvial system and preserved in the geomorphic record as terraces.

7 Conclusion

Although fluvial terraces in the Kyrgyz Tien Shan have long been linked to climate forcing and used as strain markers to determine fault-slip rates, little attention has been devoted to understanding the mechanisms by which such a complex fluvial network may generate terraces. Active tectonic structures, climate variability, and the valley-damming Beshkiol landslides (lakes 25–6 ka) combined to force geomorphic change in the Naryn River system. We aimed to disentangle these three potential drivers of alluvial terrace formation by mapping terrace profiles, and obtaining new constraints on the terrace chronology, and numerical modelling fluvial landscape change along the Naryn River system. We simulated site-specific terrace formation linked both to changing Q_s/Q_w, as a geomorphological expression of changing climate, and to base-level drop induced by lake drainage.

Despite substantial scatter in the geochronological results, they are generally consistent with the idea that climate variations explain the terrace sequences found in many tributary valleys. The most extensive terrace level throughout the region dates between 15 and 20 ka, which coincides broadly with both peak glacial extent and rapid warming as well as base-level drop after major paleo-lake drainage in the Naryn basin, suggesting that either could be responsible for the formation of this major terrace level. Mapping of tributary profiles reveals concave-up terrace profiles in their downstream reaches that would be expected from remnant depositional and aggradational features associated with lacustrine sedimentation abandoned after lake drainage. Numerical modelling of cyclic changes in the sediment-to-water ratio, in contrast, reproduces the observed spatial terrace extent in the upper tributary regions and along tributaries downstream of the landslide and the paleolake. Following these results, we consider the large Beshkiol landslide and the dammed paleo-lakes as spatially restricted drivers of terrace formation, whereas decreased Q_s/Q_w in response to reduced sediment supply following peak local LGM was the main environmental driver of terrace formation in the region. In addition to highlighting the role of specific drivers of terrace formation in the Naryn Basin, we demonstrated more broadly how modeling the long-profile evolution of alluvial networks can lend insights into the spatial distribution of terrace formation associated with a particular driver, lag times associated in terrace formation associated with given forcings, and whether modern networks might still retain signatures of ongoing transient responses.

Code and data availability

Comprehensive sample data tables, sample photos and numerical model scripts are available in the Supporting Information at https://doi.org/10.5281/zenodo.20794411 (Ruby, 2026).

https://doi.org/10.5194/egusphere-2026-3489
Preprint. Discussion started: 14 July 2026

Author contributions

Study design was developed by AR and TS. Fieldwork was conducted by AR, TS, AM and BM, while the geochronological data was processed by AR, HW, TS, TK and MF. Numerical modelling was performed by AR with contributions of FM and in discussion with AW. All co-authors contributed to editing the manuscript.

Competing interests

The contact author has declared that none of the authors has any competing interests.

Acknowledgements

We thank Julie Losen and Magali Rizza for helpful discussions.

Financial support

AR, FM, TS and AM acknowledge support from ERC Consolidator Grant 863490 GyroSCoPe, awarded to TS. AW received support from the Alexander von Humboldt Foundation via a Humboldt Research Fellowship. The development of the numerical model of channel long-profile evolution was partly supported by the National Science Foundation under Grant 1944782.

References

Abramowski, U., Bergau, A., Seebach, D., Zech, R., Glaser, B., Sosin, P., Kubik, P.W. and Zech, W.: Pleistocene glaciations of Central Asia: results from Be-10 surface exposure ages of erratic boulders from the Pamir (Tajikistan), and the Alay-Turkestan range (Kyrgyzstan), Quaternary Science Reviews, 25, https://doi.org/10.1016/j.quascirev.2005.10.003, 2006.

Attal, M. and Lavé, J.: Pebble abrasion during fluvial transport: Experimental results and implications for the evolution of the sediment load along rivers. Journal of Geophysical Research, 114(F4), https://doi.org/10.1029/2009JF001328, 2009.

Benda, L., Andras K., Miller, D. and Bigelow, P.: Confluence effects in rivers: Interactions of basin scale, network geometry, and disturbance regimes, Water Resources Research, 40, https://doi.org/10.1029/2003WR002583, 2004.

Blomdin, R., Stroeven, A. P., Harbor, J. M., Lifton, N. A., Heyman, J., Gribenski, N., Petrakov, D. A., Caffee, M. W., Ivanov, M. N., Hättestrand, C., Rogozhina, I. and Usubaliev, R.: Evaluating the timing of former glacier expansions in the Tian Shan: A key step towards robust spatial correlations, Quaternary Science Reviews, 153, 78-96. https://doi.org/10.1016/j.quascirev.2016.07.029, 2016.

Bridgland, D. and Westaway, R.: Climatically controlled river terrace staircases: A worldwide Quaternary phenomenon. Geomorphology, 98(3–4), 285–315, https://doi.org/10.1016/j.geomorph.2006.12.032, 2008.

Bull, W. B.: Geomorphic responses to climatic change, Oxford University Press, https://www.osti.gov/biblio/5603696, 1991.

Burgette, R. J., Weldon, R. J., Abdrakhmatov, K. Y., Ormukov, C., Owen, L. A. and Thompson, S. C.: Timing and process of river and lake terrace formation in the Kyrgyz Tien Shan, Quaternary Science Reviews, 159, 15-34, https://doi.org/10.1016/j.quascirev.2017.01.003, 2017.

Buylaert, J., Murray, A., Thomsen, K. and Jain, M.: Testing the potential of an elevated temperature IRSL signal from K-feldspar, Radiation Measurements, 44 (5), 560-565, https://doi.org/10.1016/j.radmeas.2009.02.007, 2009.

https://doi.org/10.5194/egusphere-2026-3489
Preprint. Discussion started: 14 July 2026

Campbell, G. E., Walker, R. T., Abdrakhmatov, K., Carolin, S., Carr, A. S., Elliott, J. R., Jackson, J., Mackenzie, D., Rizza, M., and Rodes, A.: Rapid Late Quaternary Slip, Repeated Prehistoric Earthquake Rupture, and Widespread Landsliding Associated With the Karakudzhur Thrust, Central Kyrgyz Tien Shan, Tectonics, 38(11), 3740-3764. https://doi.org/10.1029/2018tc005433, 2019.

Chen, Y., Aitchison, J. C., Zong, Y. and Li, S. H.: OSL dating of past lake levels for a large dammed lake in southern Tibet and determination of possible controls on lake evolution, Earth Surface Processes and Landforms, 41(11), 1467-1476. https://doi.org/10.1002/esp.3907, 2016.

Cheng, H., Zhang, P. Z., Spötl, C., Edwards, R. L., Cai, Y. J., Zhang, D. Z., Sang, W. C., Tan, M. and An, Z. S.: The climatic cyclicity in semiarid-arid central Asia over the past 500,000 years, Geophysical Research Letters, 39(1), https://doi.org/10.1029/2011gl050202, 2012.

Cheng, H., Spotl, C., Breitenbach, S. F., Sinha, A., Wassenburg, J. A., Jochum, K. P., Scholz, D., Li, X., Yi, L., Peng, Y., Lv, Y., Zhang, P., Votintseva, A., Loginov, V., Ning, Y., Kathayat, G. and Edwards, R. L: Climate variations of Central Asia on orbital to millennial timescales, Scientific Reports, 5, https://doi.org/10.1038/srep36975, 2016.

Clifford, N. J., Robert, A. and Richards, K. S.: Estimation of flow resistance in gravel-bedded rivers: A physical explanation of the multiplier of roughness length, Earth Surface Processes and Landforms, 17(2), 111–126. https://doi.org/10.1002/esp.3290170202, 1992.

Clubb, F. J., Mudd, S. M., Milodowski, D. T., Hurst, M. D. and Slater, L. J.: Objective extraction of channel heads from high-resolution topographic data, Water Resources Research, 50(5), 4283-4304, https://doi.org/10.1002/2013WR015167, 2014.

Coddington, J. A. and Burgette, R. J.: Fold Kinematics and Fault Slip Rates From Progressively Deformed Terraces: Implications for Structural Evolution of Basins in the Kyrgyz Tien Shan, Tectonics, 39(8). https://doi.org/10.1029/2019tc005776, 2020.

Colarossi, D., Duller, G.A.T. and Roberts, H.M.: Exploring the behaviour of luminescence signals from feldspars: Implications for the single aliquot regenerative dose protocol, Radiation Measurements 109, 35-44, https://doi.org/10.1016/j.radmeas.2017.07.005, 2018.

Colman, S. M., Karabanov, E. B. and Nelson III, C. H.: Quaternary sedimentation and subsidence history of Lake Baikal, Siberia, based on seismic stratigraphy and coring, Journal of Sedimentary Research, 73(6), 941-956, https://doi.org/10.1306/041703730941, 2003.

Cordier, S., Adamson, K., Delmas, M., Calvet, M. and Harmand, D.: Of ice and water: Quaternary fluvial response to glacial forcing, Quaternary Science Reviews, 166, 57–73, https://doi.org/10.1016/j.quascirev.2017.02.006, 2017.

Cording, A., Hetzel, R., Kober, M. and Kley, J.: ^{10}Be exposure dating of river terraces at the southern mountain front of the Dzungarian Alatau (SE Kazakhstan) reveals rate of thrust faulting over the past ~ 400 ka, Quaternary Research, 81(1), 168-178, https://doi.org/10.1016/j.yqres.2013.10.016, 2014.

Dingle, E. H., Attal, M. and Sinclair, H. D.: Abrasion-set limits on Himalayan gravel flux. Nature, 544(7651), 471-474, https://doi.org/10.1038/nature22039, 2017.

Durcan, J.A., King, G.E. and Duller, G.A.T.: DRAC: Dose Rate and Age Calculator for trapped charge dating, Quaternary Geochronology 28, 54-61, https://doi.org/10.1016/j.quageo.2015.03.012, 2015.

Exner, F. M.: Über die Wechselwirkung zwischen Wasser und Geschiebe in Flüssen, Akademie der Wissenschaften Mathematisch-Naturwissenschaftliche Klass, 134, 165–204, no DOI, 1925.

Fernandes, V. M., Ruby, A., McNab, F., Wittmann, H., Wickert, A. D., Grimm, L. and Schildgen, T. F.: Mantle-driven, climatically modulated landscape evolution in Southern Patagonia, Geology, 54(2), 117–122. https://doi.org/10.1130/G53764.1, 2025.

Fitzsimmons, K. E., Sprafke, T., Zielhofer, C., Günter, C., Deom, J.-M., Sala, R. and Iovita, R.: Loess accumulation in the Tian Shan piedmont: Implications for palaeoenvironmental change in arid Central Asia, Quaternary International, 469, 30-43, https://doi.org/10.1016/j.quaint.2016.07.041, 2018.

Fryirs, K. A., Brierley, G. J., Preston, N. J. and Spencer, J.: Catchment-scale (dis) connectivity in sediment flux in the upper Hunter catchment, New South Wales, Australia, Geomorphology, 84(3-4), 297-316, https://doi.org/10.1016/j.geomorph.2006.01.044, 2007.

Fuchs, M., Fischer, M. and Reverman, R.: Colluvial and alluvial sediment archives temporally resolved by OSL dating: Implications for reconstructing soil erosion, Quaternary Geochronology, 5 (2), 269-273, https://doi.org/10.1016/j.quageo.2009.01.006, 2010.

Galbraith, R. F., Roberts, R. G., Laslett, G. M., Yoshida, H. and Olley, J. M.: Optical dating of single and multiple grains of quartz from Jinmium rock shelter, northern Australia: Part I, experimental design and statistical models, Archaeometry 41, 339-364, https://doi.org/10.1111/j.1475-4754.1999.tb00987.x, 1999.

Gioia, D., Corrado, G., Danese, M., Minervino Amodio, A. and Schiattarella, M.: Post-lacustrine evolution of a tectonically-controlled intermontane basin: Drainage network analysis of the Mercure basin, southern Italy, Frontiers in Earth Science, 11, 1112067, https://doi.org/10.3389/feart.2023.1112067, 2023.

Gioia, D. and Schiattarella, M.: Modeling short-term landscape modification and sedimentary budget induced by dam removal: Insights from LEM application, Applied Sciences, 10(21), 7697, https://doi.org/10.3390/app10217697, 2020.

Gong, Z., Li, S.-H. and Li, B.: The evolution of a terrace sequence along the Manas River in the northern foreland basin of Tian Shan, China, as inferred from optical dating, Geomorphology, 213, 201-212, https://doi.org/10.1016/j.geomorph.2014.01.009, 2014.

Goode, J. K., Burbank, D. W. and Ormukov, C.: Pliocene-Pleistocene initiation, style, and sequencing of deformation in the central Tien Shan, Tectonics, 33(4), 464-484, https://doi.org/10.1002/2013tc003394, 2014.

Grigina, O. M. and Fortuna, A. B.: Paleogeography of the Cenozoic of the Northern Tien Shan (In Russian), Frunze (Bishkek), Ilim, 150 pp. No DOI, 1981.

Guérin, G., Mercier, N. and Adamiec, G.: Dose-rate conversion factors: update, Ancient TL 29(1), 5-8, https://doi.org/10.26034/la.atl.1998.292, 2011.

Hancock, G. S., Anderson, R. S., Chadwick, O. A. and Finkel, R. C.: Dating fluvial terraces with ^{10}Be and ^{26}Al profiles: Application to the Wind River, Wyoming, Geomorphology, 27(1–2), 41–60, https://doi.org/10.1016/S0169-555X(98)00089-0, 1999.

Harvey, A. M. and Wells, S. G.: Response of Quaternary fluvial systems to differential epeirogenic uplift: Aguas and Feos river systems, southeast Spain, Geology 15, 689–693, https://doi.org/10.1130/0091-7613(1987)15%3C689:ROQFST%3E2.0.CO;2, 1987.

Hassenruck-Gudipati, H. J., Ellis, T., Goudge, T. A. and Mohrig, D.: A multi-proxy assessment of terrace formation in the lower Trinity River valley, Texas, Earth Surface Dynamics, 10, 635–651, https://doi.org/10.5194/esurf-10-635-2022, 2022.

Hawker, L., Uhe, P., Paulo, L., Sosa, J., Savage, J., Sampson, C., and Neal, J., 2022: A 30m global map of elevation with forests and buildings removed, Environmental Research Letters, v. 17 (2), https://doi.org/10.1088/1748-9326/ac4d4f, 2022.

Hetzel, R., Niedermann, S., Tao, M., Kubik, P. W. and Strecker, M. R.: Climatic versus tectonic control on river incision at the margin of NE Tibet: ^{10}Be exposure dating of river terraces at the mountain front of the Qilian Shan, Journal of Geophysical Research, 111(F3), https://doi.org/10.1029/2005jf000352, 2006.

Holbrook, J. and Schumm, S. A.: Geomorphic and sedimentary response of rivers to tectonic deformation: a brief review and critique of a tool for recognizing subtle epeirogenic deformation in modern and ancient settings, Tectonophysics, 305(1-3), 287-306, https://doi.org/10.1016/S0040-1951(99)00011-6, 1999.

Howard, A. D.: Equilibrium and time scales in geomorphology: Application to sand-bed alluvial streams, Earth Surface Processes and Landforms, 7(4), 303–325, https://doi.org/10.1002/esp.3290070403, 1982.

Hu, Z., Pan, B., Wang, J., Cao, B. and Gao, H.: Fluvial terrace formation in the eastern Fenwei Basin, China, during the past 1.2 Ma as a combined archive of tectonics and climate change, Journal of Asian Earth Sciences, 60, 235-245, https://doi.org/10.1016/j.jseaes.2012.09.016, 2012.

Hubert-Ferrari, A.: Irregular earthquake cycle along the southern Tianshan front, Aksu area, China, Journal of Geophysical Research, 110(B6), https://doi.org/10.1029/2003jb002603, 2005.

Huffman, G. J., Stocker, E. F., Bolvin, D. T., Nelkin, E. J. and Tan, J.: GPM IMERG Final Precipitation L3 1 month 0.1 degree x 0.1 degree V07, Greenbelt, MD, Goddard Earth Sciences Data and Information Services Center (GES DISC), Accessed: [28.04.2026], 10.5067/GPM/IMERG/3B-MONTH/07, 2023.

Huntington, E.: Some characteristics of the glacial period in non-glaciated region, Bulletin of the Geological Society of America, 18(1), 351–388, https://doi.org/10.1130/gsab-18-351, 1907.

Kang, S., Roberts, H. M., Wang, X., An, Z. and Wang, M. (2015). Mass accumulation rate changes in Chinese loess during MIS 2, and asynchrony with records from Greenland ice cores and North Pacific Ocean sediments during the Last Glacial Maximum, Aeolian Research, 19, 251-258, https://doi.org/10.1016/j.aeolia.2015.05.005, 2015.

Karssenberg, D. and Bridge, J. S.: A three-dimensional numerical model of sediment transport, erosion and deposition within a network of channel belts, floodplain and hill slope: extrinsic and intrinsic controls on floodplain dynamics and alluvial architecture, Sedimentology, 55, 1717-1745, https://doi.org/10.1111/j.1365-3091.2008.00965.x, 2008.

Kolb, T., Tudyka, K., Kadereit, A., Lomax, J., Poręba, G., Zander, A., Zipf, L., and Fuchs, M.: The µDose system: determination of environmental dose rates by combined alpha and beta counting – performance tests and practical experiences, Geochronology, 4, 1–31, https://doi.org/10.5194/gchron-4-1-2022, 2022.

Koppes, M., Gillespie, A. R., Burke, R. M., Thompson, S. C. and Stone, J.: Late Quaternary glaciation in the Kyrgyz Tien Shan, Quaternary Science Reviews, 27(7-8), 846-866, https://doi.org/10.1016/j.quascirev.2008.01.009, 2008.

Korup, O., Strom, A. L. and Weidinger, J. T.: Fluvial response to large rock-slope failures: Examples from the Himalayas, the Tien Shan, and the Southern Alps in New Zealand, Geomorphology, 78(1-2), 3-21, https://doi.org/10.1016/j.geomorph.2006.01.020, 2006.

Kreutzer, S., Schmidt, C., Fuchs, M.C., Dietze, M., Fischer, M. and Fuchs, M.: Introducing an R package for luminescence dating analysis, Ancient TL, 30 (1), 1-8, https://doi.org/10.26034/la.atl.2012.457, 2012.

Lane, E. W.: The importance of fluvial morphology in hydraulic engineering, American Society of Civil Engineers Proceedings, 81(745), 1–17, no DOI, 1955.

Laskar, J., Robutel, P., Joutel, F., Gastineau, M., Correira, A. C. M. and Levrard, B.: A long-term numerical solution for the insolation quantities of the Earth, Astronomy & Astrophysics, V. 428(1), https://doi.org/10.1051/0004-6361:20041335, 2004.

Li, Y., Song, Y., Fitzsimmons, K. E., Chang, H., Orozbaev, R. and Li, X.: Eolian dust dispersal patterns since the last glacial period in eastern Central Asia: insights from a loess-paleosol sequence in the Ili Basin, Climate of the Past, 14(3), 271-286, https://doi.org/10.5194/cp-14-271-2018, 2018.

Losen, J.: Les glissements de terrain du Bassin de Naryn (Tien Shan): chronologie, impacts et implications climatiques, PhD thesis, https://doi.org/10.70675/8ee69a24z1477z422cza707z7288a508a10f, 2024.

Losen, J., Rizza, M., Nutz, A., Henriquet, M., Schuster, M., Rakhmedinov, E., Baikulov, S., Abdrakhmatov, K., Fleury, J. and Siame, L.: Repeated failures of the giant Beshkiol Landslide and their impact on the long-term Naryn Basin floodings, Kyrgyz Tien Shan, Geomorphology, 453, https://doi.org/10.1016/j.geomorph.2024.109121, 2024.

https://doi.org/10.5194/egusphere-2026-3489
Preprint. Discussion started: 14 July 2026

Lu, H., Burbank, D. W. and Li, Y.: Alluvial sequence in the north piedmont of the Chinese Tian Shan over the past 550kyr and its relationship to climate change, Palaeogeography, Palaeoclimatology, Palaeoecology, 285(3-4), 343-353. https://doi.org/10.1016/j.palaeo.2009.11.031, 2010.

Lu, H., Zhang, T., Zhao, J., Si, S., Wang, H., Chen, S., Zheng, X. and Li, Y.: Late Quaternary alluvial sequence and uplift-driven incision of the Urumqi River in the north front of the Tian Shan, northwestern China, Geomorphology, 219, 141-151, https://doi.org/10.1016/j.geomorph.2014.05.001, 2014.

Ma, Z., Peng, T., Feng, Z., Li, X., Song, C., Wang, Q., Tian, W. and Zhao, X.: Tectonic and climate controls on river terrace formation on the northeastern Tibetan Plateau: Evidence from a terrace record of the Huangshui River, Quaternary International, 656, 16-25, https://doi.org/10.1016/j.quaint.2022.11.004, 2023.

Mackenzie, D., Walker, R., Abdrakhmatov, K., Campbell, G., Carr, A., Gruetzner, C., Mukambayev, A. and Rizza, M.: A creeping intracontinental thrust fault: past and present slip-rates on the Northern edge of the Tien Shan, Kazakhstan, Geophysical Journal International, 215(2), 1148-1170, https://doi.org/10.1093/gji/ggy339, 2018.

Mackin, J. H.: Concept of the graded river. Geological Society of America Bulletin, 59(5), 463–512, https://doi.org/10.1130/0016-7606(1948)59[463:COTGR]2.0.CO;2, 1948.

Mair, D., Lechmann, A., Delunel, R., Yeşilyurt, S., Tikhomirov, D., Vockenhuber, C., Christl, M., Akcar, N. and Schlunegger, F.: The role of frost cracking in local denudation of steep Alpine rockwalls over millennia (Eiger, Switzerland), Earth Surface Dynamics, 8(3), 637-659, https://doi.org/10.5194/esurf-8-637-2020, 2020.

Malatesta, L. C., Avouac, J.-P., Brown, N. D., Breitenbach, S. F. M., Pan, J., Chevalier, M.-L., Rhodes, E., Saint-Carlier, D., Zhang, W., Charreau, J., Lavé, J. and Blard, P.-H.: Lag and mixing during sediment transfer across the Tian Shan piedmont caused by climate-driven aggradation-incision cycles, Basin Research, 30(4), 613-635, https://doi.org/10.1111/bre.12267, 2018.

Marshall, J. A., Roering, J. J., Bartlein, P. J., Gavin, D. G., Granger, D. E., Rempel, A. W., Praskievicz, S. J. and Hales, T. C.: Frost for the trees: Did climate increase erosion in unglaciated landscapes during the late Pleistocene? Science Advances, 1(10), https://doi.org/10.1126/sciadv.1500715, 2015.

Martin, L. C. P., Blard, P. H., Balco, G., Lavé, J., Delunel, R., Lifton, N. and Laurent, V.: The CREp program and the ICE-D production rate calibration database: a fully parameterizable and updated online tool to compute cosmic-ray exposure ages, Quaternary Geochronology, v. 38, pp. 25–49, doi:10.1016/j.quageo.2016.11, 2017.

McGregor, I. S. and Onderdonk, N. W.: Late Pleistocene rates of rock uplift and faulting at the boundary between the southern Coast Ranges and the western Transverse Ranges in California from reconstruction and luminescence dating of the Orcutt Formation, Geosphere, 17(3), 932-956, https://doi.org/10.1130/GES02274.1, 2021.

McNab, F., Schildgen, T. F., Turowski, J. M. and Wickert, A. D.: Diverse Responses of Alluvial Rivers to Periodic Environmental Change, Geophysical Research Letters, 50(10), https://doi.org/10.1029/2023gl103075, 2023.

McNab, F., Schildgen, T. F., Turowski, J. M., & Wickert, A. D.: Influence of network geometry on long-term morphodynamics of alluvial rivers, Earth Surface Dynamics, 13(5), 1059-1092, https://doi.org/10.5194/esurf-13-1059-2025, 2025.

Merritts, D. J., Vincent, K. R. and Wohl, E. E.: Long river profiles, tectonism, and eustasy: A guide to interpreting fluvial terraces, Journal of Geophysical Research: Solid Earth, 99(B7), 14031-14050, https://doi.org/10.1029/94JB00857, 1994.

Meyer-Peter, E. and Müller, R.: Formulas for bed-load transport. In Proceedings of the 2nd meeting of the International Association for Hydraulic Structures Research, 39–64, no DOI, 1948.

Molnar, P., Brown, E. T., Burchfiel, B. C., Deng, Q., Feng, X., Li, J., Raisbeck, G. M., Shi, J., Zhangming, W. and Yiou, F.: Quaternary climate change and the formation of river terraces across growing anticlines on the

https://doi.org/10.5194/egusphere-2026-3489
Preprint. Discussion started: 14 July 2026

north flank of the Tien Shan, China, The Journal of Geology, 102(5), 583-602, https://doi.org/10.1086/629700, 1994.

Narama, C., Kondo, R., Tsukamoto, S., Kajiura, T., Ormukov, C. and Abdrakhmatov, K.: OSL dating of glacial deposits during the last glacial in the Terskey-Alatoo range, Kyrgyz Republic, Quaternary Geochronology, 2, https://doi.org/10.1016/j.quageo.2006.06.007, 2007.

Narama, C., Kondo, R., Tsukamoto, S., Kajiura, T., Duishonakunov, M. and Abdrakhmatov, K.: Timing of glacier expansion during the last glacial in the inner Tien Shan, Kyrgyz Republic by OSL dating, Quaternary International, 199 (1), https://doi.org/10.1016/j.quaint.2008.04.010, 2009.

Nishiizumi, K., Imamura, M., Caffee, M.W., Southon, J.R., Finkel, R.C. and McAninch, J.: Absolute calibration of 10Be AMS standards: Nuclear Instruments and Methods in Physics Research Section B, Beam Interactions with Materials and Atoms, 258 (2), 403–413, https://doi.org/10.1016/j.nimb.2007.01.297, 2007.

O'Connell, D. R. and Turner, J.: Hosgri fault transpressional slip rates reproduce observed Central California coast uplift rates, The Seismic Record, 3(3), 182-193, https://doi.org/10.1785/0320220047, 2023.

Ouchi, S.: Response of alluvial rivers to slow active tectonic movement, Geological Society of America Bulletin, 96(4), 504-515, https://doi.org/10.1130/0016-7606(1985)96%3C504:ROARTS%3E2.0.CO;2, 1985.

Paola, C., Hellert, P. L. and Angevinet, C. L.: The large-scale dynamics of grain-size variation in alluvial basins, 1: Theory, Basin Research, 4, 73-90, https://doi.org/10.1111/j.1365-2117.1992.tb00145.x, 1992.

Parker, G.: Self-formed straight rivers with equilibrium banks and mobile bed. Part 2. The gravel river, Journal of Fluid Mechanics, 89(1), 127–146, https://doi.org/10.1017/S0022112078002505, 1978.

Parker, G.: Downstream variation of grain size in gravel rivers: Abrasion versus selective sorting, In A. Armanini and G. Di Silvio (Eds.): Fluvial hydraulics of Mountain regions, lecture notes in Earth sciences, 37, 345–360, Springer, https://doi.org/10.1007/BFb0011201, 1991.

Pazzaglia, F. J.: 9.23 Fluvial terraces, In E. Wohl (Ed.), Treatise of geomorphology, 379–412, Elsevier, https://doi.org/10.1016/B978-0-12-374739-6.00248-7, 2013.

Penprase, S. B., Wickert, A. D., Larson, P. H., Wood, J. J., Larsen, I. J. and Rittenour, T. M.: Plow versus Ice Age: Erosion rate variability from glacial- interglacial climate change is an order of magnitude lower than agricultural erosion in the Upper Mississippi River Valley, USA, Geology, 53(6), 535–539, https://doi.org/10.1130/G52585.1, 2025.

Poisson, B. and Avouac, J.-P.: Holocene hydrological changes inferred from alluvial stream entrenchment in north Tian Shan (northwestern China), The Journal of Geology, 112(2), 231–249, https://doi.org/10.1086/381659, 2004.

Prescott, J. R. and Hutton, J. T.: Cosmic ray contributions to dose rates for luminescence and ESR dating: large depth and long-term time variations, Radiation Measurements 23, 497-500, https://doi.org/10.1016/1350-4487(94)90086-8, 1994.

Roda-Boluda, D. C., Schildgen, T. F., Wittmann, H., Tofelde, S., Bufe, A., Prancevic, J. and Hovius, N.: Elevation-dependent periglacial and paraglacial processes modulate tectonically-controlled erosion of the western Southern Alps, New Zealand, Journal of Geophysical Research: Earth Surface, 128(11), https://doi.org/10.1029/2023JF007271, 2023.

Ruby, A.: Supplement to: "Climatic, tectonic and landslide-dam signals preserved in alluvial terraces of the Naryn Basin, Kyrgyzstan" by Ruby et al. [Supplementary Information]. Zenodo, https://doi.org/10.5281/zenodo.20794411, 2026.

Ruby, A., McNab, F., Schildgen, T. F., Wickert, A. D. and Fernandes, V. M.: How sediment supply, sea-level, and glacial isostatic oscillations drive alluvial river long-profile evolution and terrace formation, AGU Advances, 7, https://doi.org/10.1029/2025AV002035, 2026.

Rust, B. R.: Sedimentation in fluvial and lacustrine environments, Hydrobiologia, 91(1), 59-70, no DOI, 1982.

https://doi.org/10.5194/egusphere-2026-3489
Preprint. Discussion started: 14 July 2026

Saint-Carlier, D., Charreau, J., Lavé, J., Blard, P.-H., Dominguez, S., Avouac, J.-P. and Wang, S.: Major temporal variations in shortening rate absorbed along a large active fold of the southeastern Tianshan piedmont (China), Earth and Planetary Science Letters, 434, 333-348, https://doi.org/10.1016/j.epsl.2015.11.041, 2016.

Savi, S., Tofelde, S., Wickert, A. D., Bufe, A., Schildgen, T. F. and Strecker, M. R.: Interactions between main channels and tributary alluvial fans: channel adjustments and sediment-signal propagation, Earth Surface Dynamics, 8(2), 303-322, https://doi.org/10.5194/esurf-8-303-2020, 2020.

Scharer, K. M., Burbank, D. W., Chen, J. and Weldon, R. J.: Kinematic models of fluvial terraces over active detachment folds: Constraints on the growth mechanism of the Kashi-Atushi fold system, Chinese Tian Shan, Geological Society of America Bulletin, 118(7-8), 1006-1021, https://doi.org/10.1130/b25835.1, 2006.

Scherler, D., Bookhagen, B., Wulf, H., Preusser, F. and Strecker, M. R.: Increased late Pleistocene erosion rates during fluvial aggradation in the Garhwal Himalaya, northern India, Earth and Planetary Science Letters, 428, 255–266, https://doi.org/10.1016/j.epsl.2015.06.034, 2015.

Schumm, S. A.: Geomorphic thresholds and complex response of drainage systems, Fluvial geomorphology, 6, 69-85, no DOI, 1973.

Schwanghart, W. and Scherler, D.: TopoToolbox 2–MATLAB-based software for topographic analysis and modeling in Earth surface sciences, Earth Surface Dynamics, 2(1), 1-7, https://doi.org/10.5194/esurf-2-1-2014, 2014.

Selander, J., Oskin, M., Ormukov, C. and Abdrakhmatov, K.: Inherited strike-slip faults as an origin for basement-cored uplifts: Example of the Kungey and Zailiskey ranges, northern Tian Shan, Tectonics, 31(4), n/a-n/a. https://doi.org/10.1029/2011tc003002, 2012.

Song, Y., Zeng, M., Chen, X., Li, Y., Chang, H., An, Z. and Guo, X.: Abrupt climatic events recorded by the Ili loess during the last glaciation in Central Asia: Evidence from grain-size and minerals, Journal of Asian Earth Sciences, 155, 58-67, https://doi.org/10.1016/j.jseaes.2017.10.040, 2018.

Stokes, M. and Mather, A.E.: Response of Plio-Pleistocene alluvial systems to tectonically induced base-level changes, Vera Basin, SE Spain, Journal of the Geological Society (London) 157, 303–316, https://doi.org/10.1144/jgs.157.2.303, 2000.

Strom, A. L.: Giant ancient rock slides and rock avalanches in the Tien Shan Mountains, Kyrgyzstan, Landslide News 11, 20–23. No DOI, 1998.

Thomsen, K., Murray, A., Jain, M. and Bøtter-Jensen, L.: Laboratory fading rates of various luminescence signals from feldspar-rich sediment extracts, Radiation Measurements, 43 (9), 1474-1486, https://doi.org/10.1016/j.radmeas.2008.06.002, 2008.

Thompson, S. C., Weldon, R. J., Rubin, C. M., Abdrakhmatov, K., Molnar, P. and Berger, G. W.: Late Quaternary slip rates across the central Tien Shan, Kyrgyzstan, central Asia, Journal of Geophysical Research: Solid Earth, 107(B9), 7-32, https://doi.org/10.1029/2001jb000596, 2002.

Tofelde, S., Schildgen, T. F., Savi, S., Pingel, H., Wickert, A. D., Bookhagen, B., Wittmann, H., Alonso, R. N., Cottle, J. and Strecker, M. R.: 100 kyr fluvial cut-and-fill terrace cycles since the Middle Pleistocene in the southern Central Andes, NW Argentina, Earth and Planetary Science Letters, 473, 141-153, https://doi.org/10.1016/j.epsl.2017.06.001, 2017.

Tofelde, S., Savi, S., Wickert, A. D., Bufe, A. and Schildgen, T. F.: Alluvial channel response to environmental perturbations: fill-terrace formation and sediment-signal disruption, Earth Surface Dynamics, 7(2), 609-631, https://doi.org/10.5194/esurf-7-609-2019, 2019.

Torres Acosta, V., Schildgen, T. F., Clarke, B. A., Scherler, D., Bookhagen, B., Wittmann, H., von Blanckenburg, F. and Strecker, M. R.: Effect of vegetation cover on millennial-scale landscape denudation rates in East Africa, Lithosphere, 7(4), 408-420, https://doi.org/10.1130/L402.1, 2015.

https://doi.org/10.5194/egusphere-2026-3489
Preprint. Discussion started: 14 July 2026

Tudyka K., Bluszcz, A., Poreba, G., Miaosz, S., Adamiec, G., Kolarczyk, A., Kolb, T., Lomax, J. and Fuchs, M.: Increased dose rate precision in combined α and β counting in the μDose system - a probabilistic approach to data analysis, Radiation Measurements, 134, https://doi.org/ 10.1016/j.radmeas.2020.106310, 2020.

Viveen, W., Schoorl, J. M., Veldkamp, A. and van Balen, R. T.: Modelling the impact of regional uplift and local tectonics on fluvial terrace preservation, Geomorphology, 210, 119-135, https://doi.org/10.1016/j.geomorph.2013.12.026, 2014.

van den Berg van Saparoea, A.-P. H. and Postma, G.: Control of climate change on the yield of river systems. In Hampson, G. J., Steel, R. J., Burgess, P. M. and Dalrymple, R. W.: Recent Advances in Models of Siliciclastic Shallow-Marine Stratigraphy, Society for Sedimentary Geology, https://doi.org/10.2110/pec.08.90.0015, 2008.

Vandenberghe, J.: Climate forcing of fluvial system development: An evolution of ideas, Quaternary Science Reviews, 22(20), 2053–2060, https://doi.org/10.1016/s0277-3791(03)00213-0, 2003.

Vandenberghe, J.: The fluvial cycle at cold–warm–cold transitions in lowland regions: A refinement of theory, Geomorphology, 98(3–4), 275–284, https://doi.org/10.1016/j.geomorph.2006.12.030, 2008.

von Blanckenburg, F., Hewawasam, T. and Kubik, P.W.: Cosmogenic nuclide evidence for low weathering and denudation in the wet, tropical highlands of Sri Lanka, Journal of Geophysical Research, 109, https://doi.org/10.1029/2003JF000049, 2004.

Wells, J. T., Scholz, C. A. and Soreghan, M. J.: Processes of sedimentation on a lacustrine border-fault margin; interpretation of cores from Lake Malawi, East Africa, Journal of Sedimentary Research, 69(4), 816-831, https://doi.org/10.2110/jsr.69.816, 1999.

Wickert, A. D., McNab, F. and Barefoot, E.: GRLP (v2.0.0) [Software], Zenodo, https://doi.org/10.5281/zenodo.17091246, 2025.

Wickert, A. D. and Schildgen, T. F.: Long-profile evolution of transport-limited gravel-bed rivers, Earth Surface Dynamics, 7(1), 17-43, https://doi.org/10.5194/esurf-7-17-2019, 2019.

Wong, M. and Parker, G.: Reanalysis and correction of bed-load relation of Meyer-Peter and Müller using their own database, Journal of Hydraulic Engineering, 132(11), 1159–1168, https://doi.org/10.1061/(ASCE)0733-9429(2006)132:11(1159), 2006.

Yang, X., Li, A. and Hunag, W.: Uplift differential of active fold zones during the late Quaternary, northern piedmonts of the Tianshan Mountains, China, Science China Earth Sciences, 56(5), 794-805, https://doi.org/10.1007/s11430-012-4531-z, 2013.

Youn, J. H., Seong, Y. B., Choi, J. H., Abdrakhmatov, K. and Ormukov, C.: Loess deposits in the northern Kyrgyz Tien Shan: Implications for the paleoclimate reconstruction during the Late Quaternary, Catena, 117, 81-93, https://doi.org/10.1016/j.catena.2013.09.007, 2014.

Zhao, J., Song, Y., King, J. W., Liu, S., Wang, J. and Wu, M.: Glacial geomorphology and glacial history of the Muzart River valley, Tianshan range, China, Quaternary Science Review, 29 (11), https://doi.org/10.1016/j.quascirev.2010.03.004, 2010.

Zech, R.: A late Pleistocene glacial chronology from the Kitschi-Kurumdu Valley, Tien Shan (Kyrgyzstan), based on ^{10}Be surface exposure dating, Quaternary Research, 77 (2), https://doi.org/10.1016/j.yqres.2011.11.008, 2012.

Zech, C., Schöne, T., Illigner, J., Stolarczuk, N., Queißer, T., Köppl, M., Thoss, H., Zubovich, A., Sharshebaev, A., Zakhidov, K., Toshpulatov, K., Tillayev, Y., Olimov, S., Paiman, Z., Unger-Shayesteh, K., Gafurov, A. and Moldobekov, B.: Hydrometeorological data from a Remotely Operated Multi-Parameter Station network in Central Asia, Earth System Science Data, 13, 1289–1306, https://doi.org/10.5194/essd-13-1289-2021, 2021.

https://doi.org/10.5194/egusphere-2026-3489
Preprint. Discussion started: 14 July 2026

Zelenin, E., Bachmanov, D., Garipova, S., Trifonov, V. and Kozhurin, A.: The Active Faults of Eurasia Database (AFEAD): the ontology and design behind the continental-scale dataset, Earth System Science Data, 14, 4489–4503, https://doi.org/10.5194/essd-14-4489-2022, 2022.

Zhang, J., Xu, B., Gu, Z., Lv, Y., Yin, Z., Guo, X. and Li, L.: Coupling of river discharges and alpine glaciers in arid Central Asia, Quaternary International, 667, 19-28. https://doi.org/10.1016/j.quaint.2023.06.002, 2023.